*Electronic Supplementary Material (**ESI**) for*

Tunable Reversible Metallo-hydrogels: A New platform for Visual Discrimination of Biothiols

*Weiwei Fang, Cong Liu, Zhengwei Lu, Zheming Sun and Tao Tu**

Department of Chemistry, Fudan University

220 Handan Road, Shanghai, 200433, China

E-mail: taotu@fudan.edu.cn

Table of Contents:

1. General.

All commercial reagents and solvents were used directly without further purification. ^{1}H and ^{13}C NMR were recorded on Jeol ECA-400 and Bruker 500 DRX spectrometers. ESI-MS spectra were recorded on a Bruker micrOTOF II instrument. Powder X-ray diffraction (PXRD) patterns were measured using a Bruker D8 powder diffractometer with Cu Kα radiation (λ = 1.5406 Å). Data collections were carried out on a Bruker Smart APEX diffractometer equipped with a normal focus, 2.4 kW sealed tube X-ray source (Mo Kα radiation, λ= 0.71073 Å) operating at 50 kV and 30 mA at 293 K. SEM experiments were carried out on a Philips XL30 microscope operated at 20 kV. All reactions were carried out under air unless otherwise noted. Rheological measurements were carried out on freshly prepared gels using a controlled stress rheometer (Malvern Bohlin Gemini HR nano).

2. Experimental techniques.

2.1 **Gelation test.**

For the preparation of the metallogel samples, the solvents were used as purchased. For 0.4 wt% gel: 10 mg complex **2** with/without 2 eq. amino acids were filled into a screw-cap vial and then solvent (2.5 mL) was added by syringe. The exact concentration was determined by differential weighting. The Zn(II)-pincer complex was dissolved by heating with a heat-gun or continuous shaking. Then, the samples were allowed to cool down slowly or rest at room temperature to test if a gel was formed.

2.2 **Determination of gel-to-solution phase-transition temperatures T_g by using a test-tube-inversion method.**[S1]

A vial containing the gel sample was immersed inversely in a thermostat controlled oil bath and the temperature was raised at a rate of 0.5 °C per minute. The T_g was defined as the temperature at which the gel collapsed.

2.3 **Scanning electron microscopy (SEM).**

SEM experiments were carried out on a Philips XL30 microscope operated at 20 kV. All pictures were taken digitally. For preparation of the samples, a silicon sheet was placed on the surface of the gel for a short time. The gel samples were partly destroyed by knocking the test tube on the table to provide a "print" of the inner volume of the gel.

2.4 **Rheology**

Rheological measurements were carried out on freshly prepared gels using a controlled stress rheometer (Malvern Bohlin Gemini HR nano). Cone and plate geometry of 40 mm diameter was employed throughout the dynamic oscillatory work. The following tests were performed: increasing amplitude of oscillation up to 100% apparent strain shear (kept at a frequency of 6.283 rad s^{-1}) and frequency sweeps at 25 ^{o}C (from 10– 0.001 rad s^{-1}, 0.8% strain).

2.5 **X-ray scattering (SAXS)**

Characterization with *X-rays* was performed using a pinhole camera with a rotating anode generator (Cu Kα radiation from crossed Göbel mirrors by using Bruker AXS D8 with a power of 40 kV and 50 mA). All X-ray patterns were radially averaged and corrected for background scattering from the solvent to obtain the scattering intensity in dependence on the scattering vector $q = (4/\pi)\sin\theta$, with 2θ being the scattering angle and λ = 0.15406 nm as the X-ray wavelength**.**

3. Synthesis of Zn(II)-pincer complex 2.

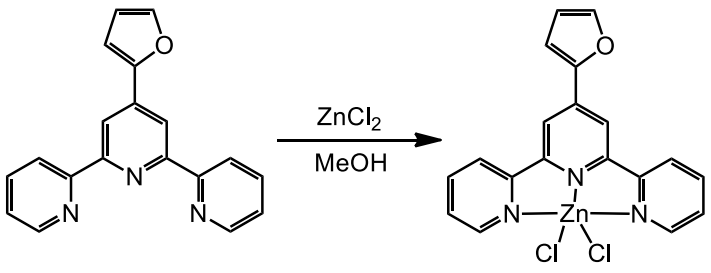

1 **2**

Scheme S1. Synthesis of Zn(II)-pincer complex **2**.

Terpyridine **1**[S2] (898 mg, 3 mmol) and $ZnCl_2$ (491 mg, 3.6 mmol) were added into MeOH (90 mL), which were further stirred at room temperature for 24 h. The white solid was collected through filtration, washed with MeOH (30 mL) three times and then dried under vacuum to give complex **2** as a white solid (396 mg, 91%). ^{1}H NMR (DMSO-D_6, 400 MHz, 298 K): δ = 8.87 (s, 2H), 8.81-8.77 (m, 4H), 8.28 (t, *J* = 7.2 Hz, 2H), 8.07 (s, 1H), 7.85 (t, *J* = 7.2 Hz, 2H), 7.77 (d, *J* = 2.4 Hz, 1H), 6.80 (d, *J* = 1.2 Hz, 1H); ^{13}C NMR (DMSO-D_6, 100 MHz, 298 K) δ = 149.06, 148.78, 148.49, 146.53, 142.81, 140.32, 127.06, 122.07, 115.59, 113.98, 113.17; HR-MS (ESI): m/z 455.9625 (Calcd. $[M+Na]^+$), 455.9614 (Found. $[M+Na]^+$); 398.0039 (Calcd. $[M-Cl]^+$), 398.0024 (Found. $[M-Cl]^+$).

4. Chemical structures of amino acids and other mercapto molecules.

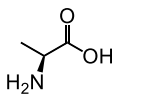

L-Alanine
(L-Ala)

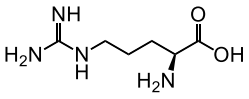

L-Arginine
(L-Arg)

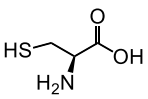

L-Cysteine
(L-Cys)

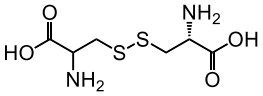

L-Cystine

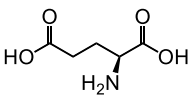

L-Glutaminic acid
(L-Glu)

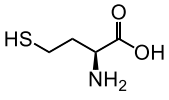

L-Homocysteine
(L-Hcy)

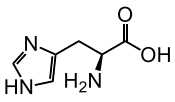

L-Histidine
(L-His)

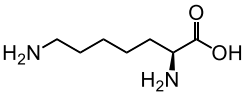

L-Lysine
(L-Lys)

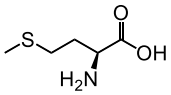

L-Methionine
(L-Met)

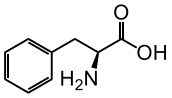

D-Phenylalanine
(D-Phe)

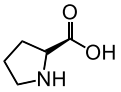

L-Proline
(L-Pro)

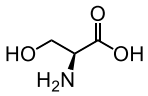

L-Serine
(L-Ser)

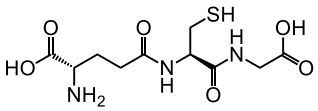

Glutathione
(GSH)

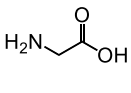

Glycine
(Gly)

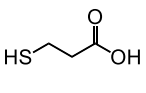

3-Mercaptopropionic acid
(3-MPA)

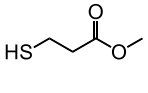

Methyl 3-Mercaptopropionate
(3-MPE)

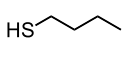

Butyl Mercaptan

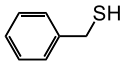

Benzyl mercaptan

5. Gelation tests of complex 2 in various organic solvents.

Table S1. Gelation ability of complex **2** in various solvents.[a]

Solvent	Phase	Solvent	Phase
H_2O	P	DMSO	S
H_2O	P[b]	DMF	P
H_2O	P[c]	DMA	P
H_2O	S[d]	NMP	S
MeOH	P	Toluene	I
EtOH	I	Benzene	I
n-PrOH	I	PhCl	I
i-PrOH	I	Pyridine	S
n-BuOH	I	PhCN	P
t-BuOH	I	ACN	I
1,2-Ethanediol	P	THF	I
1,3-Propanediol	P	Dioxane	I
1,4-Butanediol	PG	DME	I
Glycerin	G	DCM	I
Triglycol	P	TCM	I
Polyethylene glycol	S	DCE	I
AcOH	I	EA	I
Acetone	I	PE	I

[a] Gelator concentration: 1 wt%; G: gel; PG: partial gel; P: precipitate; S: soluble; I: insoluble. [b] Gelator concentration: 0.5 wt%. [c] Gelator concentration: 0.4 wt%. [d] Gelator concentration: 0.3 wt%.

***Table S2*.** Gelation ability of complex **2** with additives in H_2O.[a]

Entry	Additive (2 eq.)	Phase	T_g [^oC]
1	L-Ala	P	/
2	L-Arg	P	/
3	L-Cys	G/WG[b]	33.8
4	L-Cystine	P	/
5	L-Glu	P	/
6	L-Hcy	G	47.0
7	L-His	S	/
8	L-Lys	P	/
9	L-Met	P	/
10	D-Phe	P	/
11	L-Pro	P	/
12	L-Ser	P	/
13	GSH	G[c]	30.0
14	Gly	P	/
15	3-MPA	G	46.4
16	3-MPAE	G	42.7
17	Butyl Mercaptan	G	30.8
18	Benzyl mercaptan	P	/

[a] Gelator concentration: 0.4 wt%; G: gel; WG: weak gel; S: soluble; P: precipitate. [b] 1 eq. L-Cys. [c] Gelator concentration: 0.48 wt%.

6. Sol-gel transition temperatures (T_g) for metallo-hydrogels.

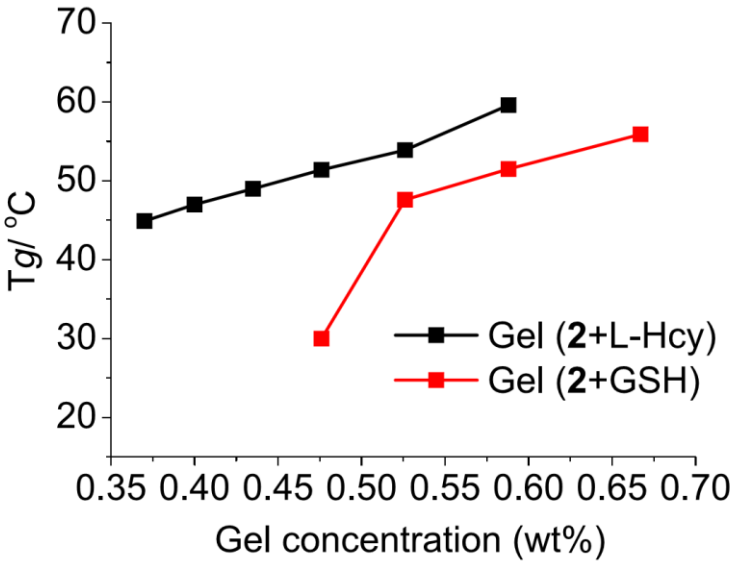

Figure S1. Sol-gel transition temperatures (T_g) for metallo-hydrogels of [**2**+Hcy] and [**2**+GSH] as a function of gelator concentrations.

7. Selective metallo-hydrogel formation by complex 2 and L-Cys.

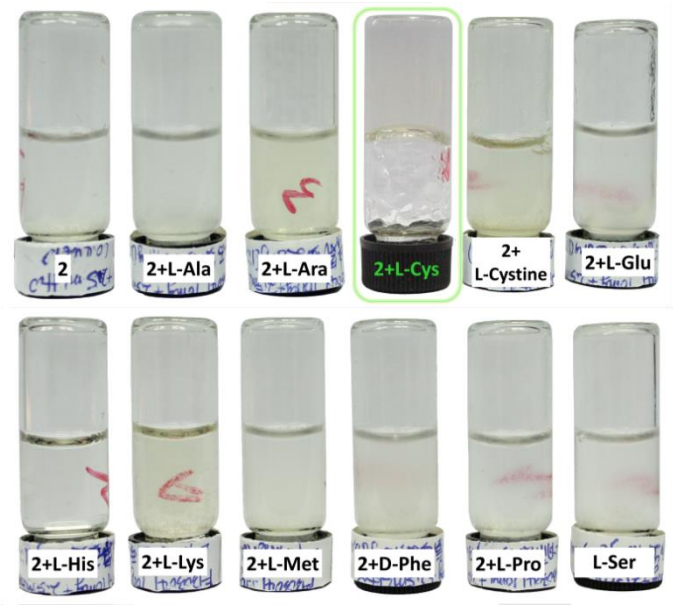

Figure S2. Selective metallogel formation by complex **2** and L-Cys after heating/cooling procedure in H_2O.

8. Visual discrimination of L-Hcy from L-Cys and GSH through metallo-hydrogel reformation.

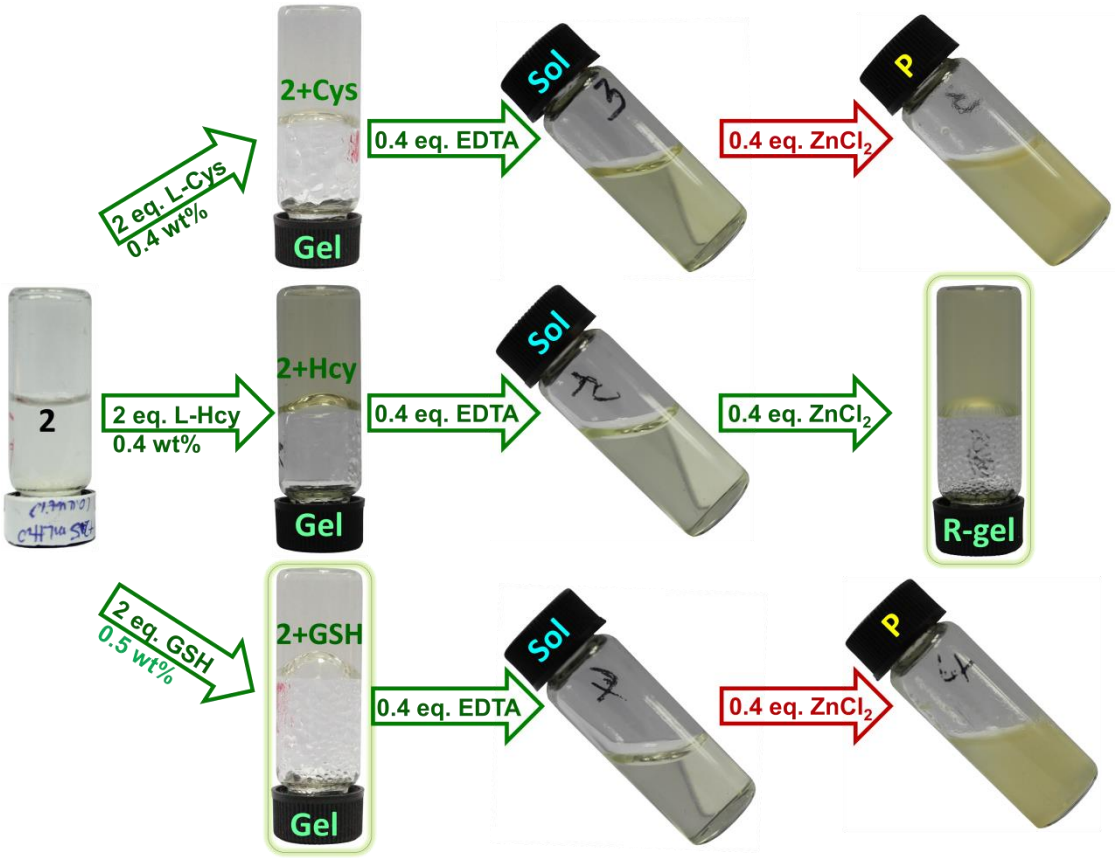

Figure S3. Visual discrimination of L-Hcy from L-Cys and GSH *via* a selective metallo-hydrogel gelation, sol formation and regelation sequence.

9. Temperature-dependent ^{1}H NMR study.

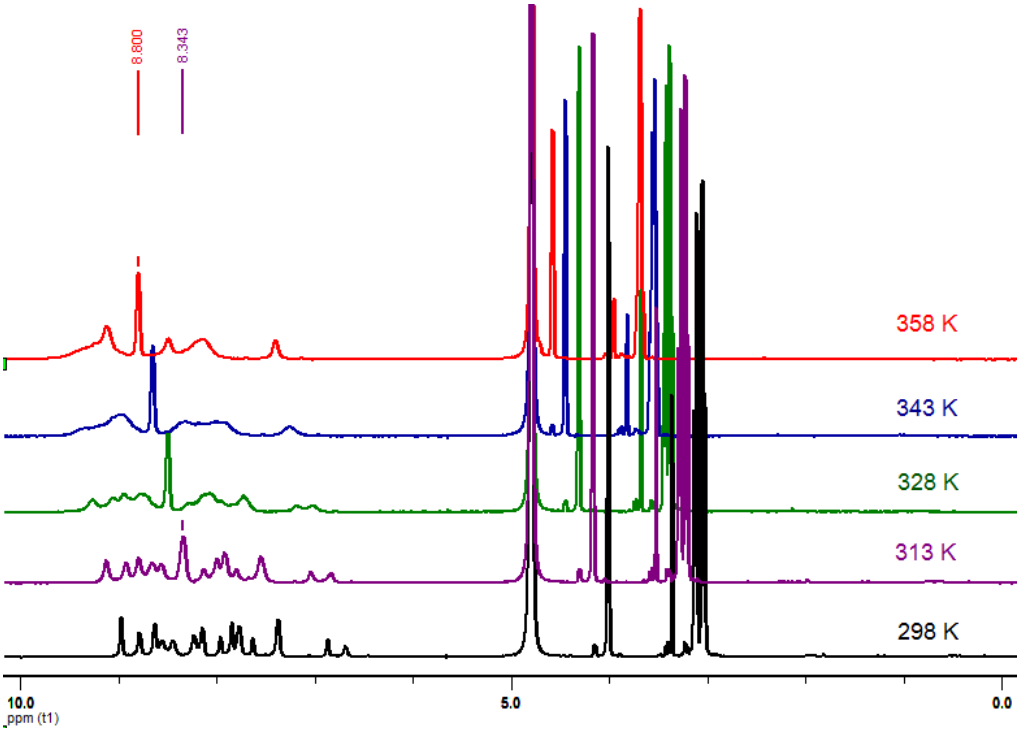

Figure S4. Temperature-dependent ^{1}H NMR spectra of metallo-gel [**2**+Cys]/D_2O (0.67 wt %).

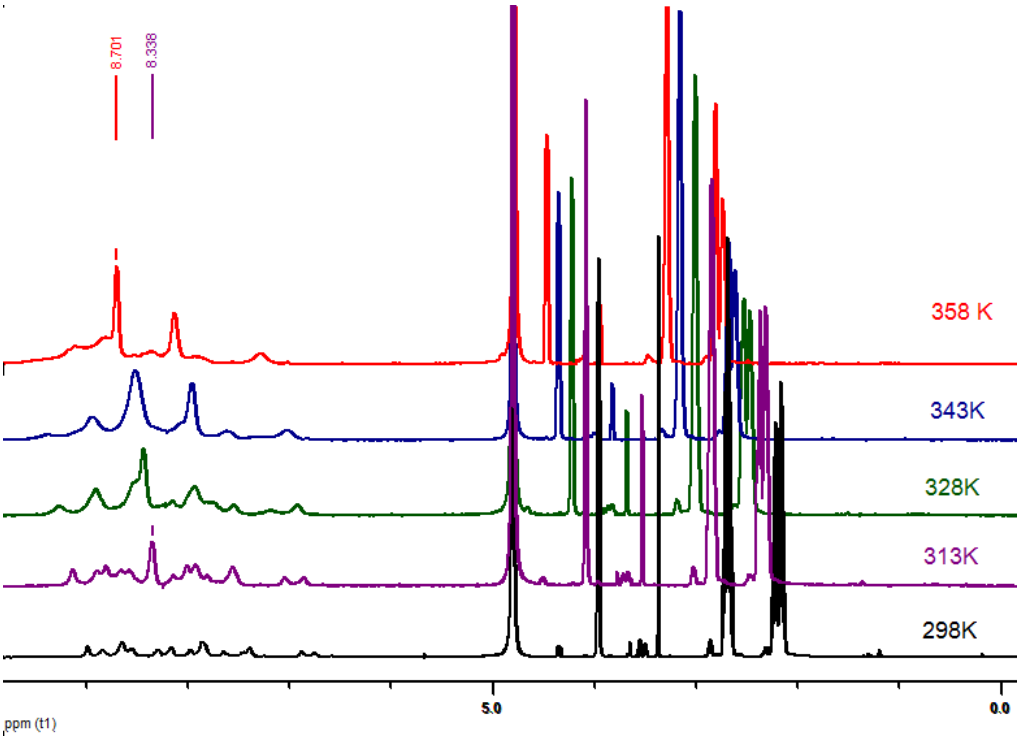

Figure S5. Temperature-dependent ^{1}H NMR spectra of metallo-gel [**2**+Hcy]/D_2O (0.67 wt %).

10. X-Ray diffraction (XRD) study.

The structure and dimension of the xerogel networks of [**2**+Hcy] and [**2**+Cys] (0.5 wt %) were studied by X-ray diffraction, and the results provided further support for π−π stacking and metal−metal interactions between the coplanar hetero-aromatic rings of the pincer ligands in complex **2** as major contributions to the gelation process (Fig. S6 and S7). A major absorption in the XRD pattern of xerogel [**2**+Hcy] appeared at 2θ = 26.88 (d_{001}) indicating a typical distance of 3.31 Å, which is slightly shorter than that founded in the xerogel [**2**+Cys] (3.41 Å). And stronger interactions may exist in the gels [**2**+Hcy] than [**2**+Cys], which was in accordance with the results observed from T_g study.

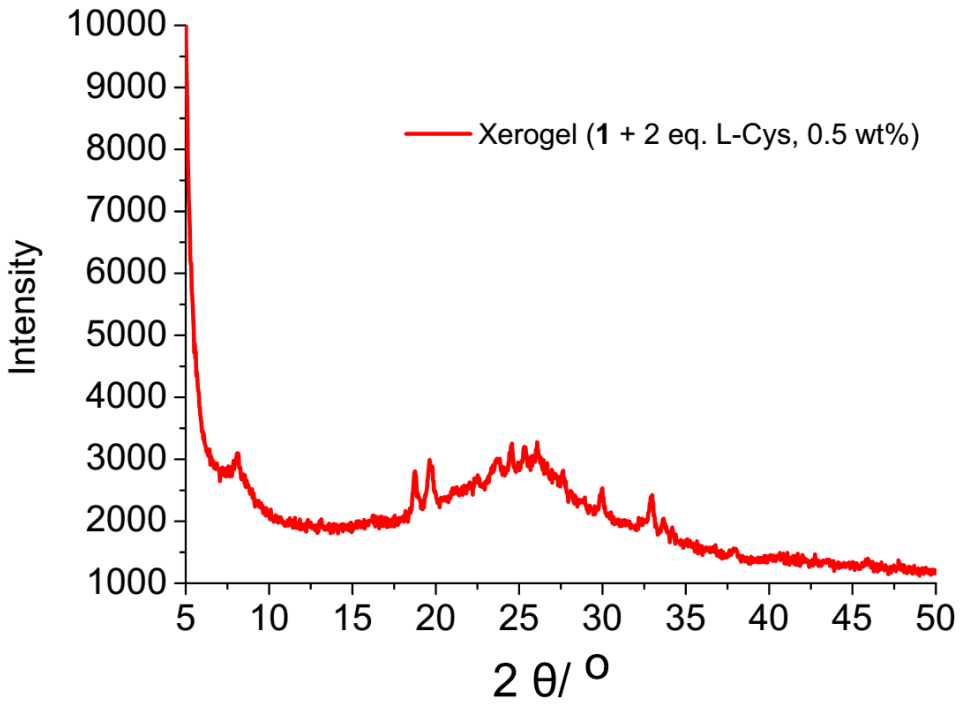

Figure S6. X-Ray diffraction pattern of xerogel [**2**+Cys]/D_2O (0.5 wt%).

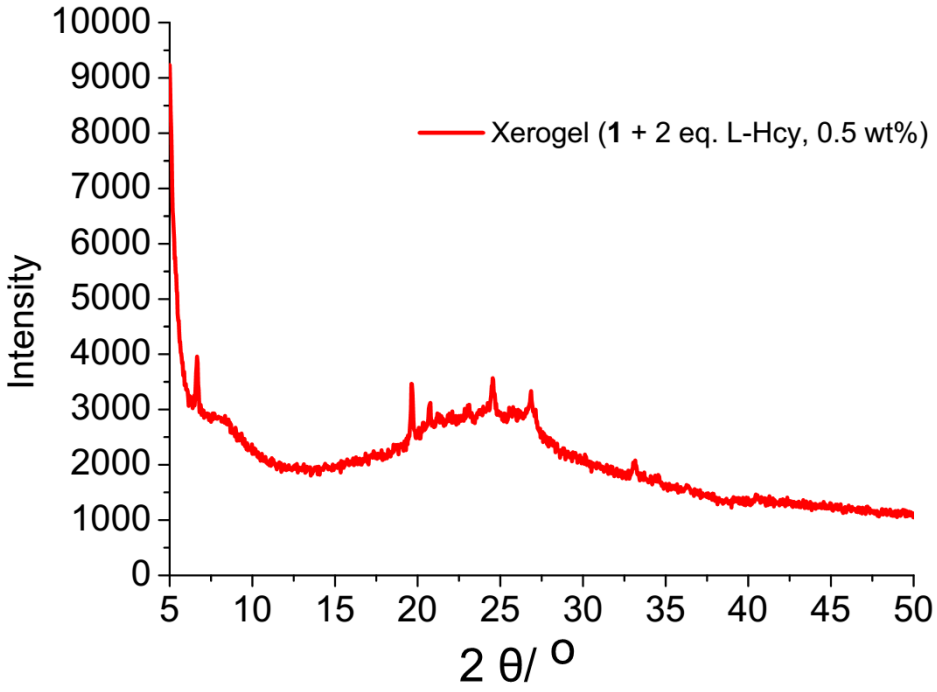

Figure S7. X-Ray diffraction pattern of xerogel [**2**+Hcy]/D_2O (0.5 wt%).

11. Rheology study of metallo-hydrogels.

In order to quantify the thixotropic behaviors and the selective gel reformation ability, a series of rheological studies were carried out with 0.42 wt% gels [**2**+Cys]/H_2O and [**2**+Hcy]/H_2O.[S3] Consistent with shear strain tests, the gel [**2**+Hcy]/H_2O revealed a greater elastic storage modulus (G', ca. 3.7 Pa) than that of gel [**2**+Cys] /H_2O at the same concentration (G', 1.3 Pa). Due to the low gelator concentration, both values were relatively low (Fig. S8 and S10). Dynamic frequency sweep studies reveal that the viscosities (η*) of metallo-hydrogels decreased with the increasing frequency and demonstrated the shearing thinning phenomena which further confirms the thixotropic character of the hydrogels (Fig. S9 and S11). Both T_g and rheological studies characterize gel [**2**+Hcy]/H_2O as stronger thixotropic than gel [**2**+Cys]/H_2O, a result suited to guide us in our attempt to design a proper chemo-switch.

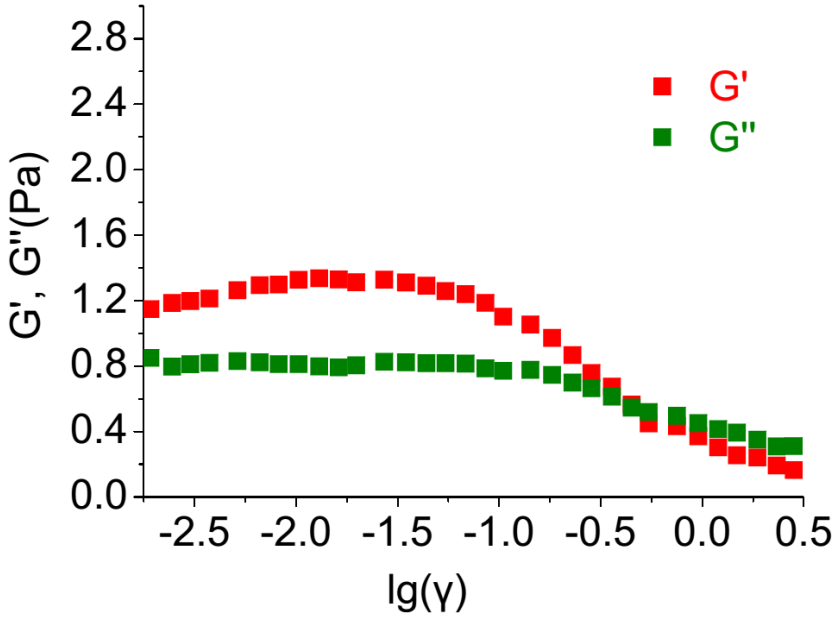

Figure S8. Amplitude sweep rheometry data (storage modulus G' and loss modulus G'' *vs.* shear strain γ) for metallo-hydrogel [**2**+Cys] (0.5 wt%) at 25 °C (angular frequency: 6.283 rad s¯1, strain: 0.001–10).

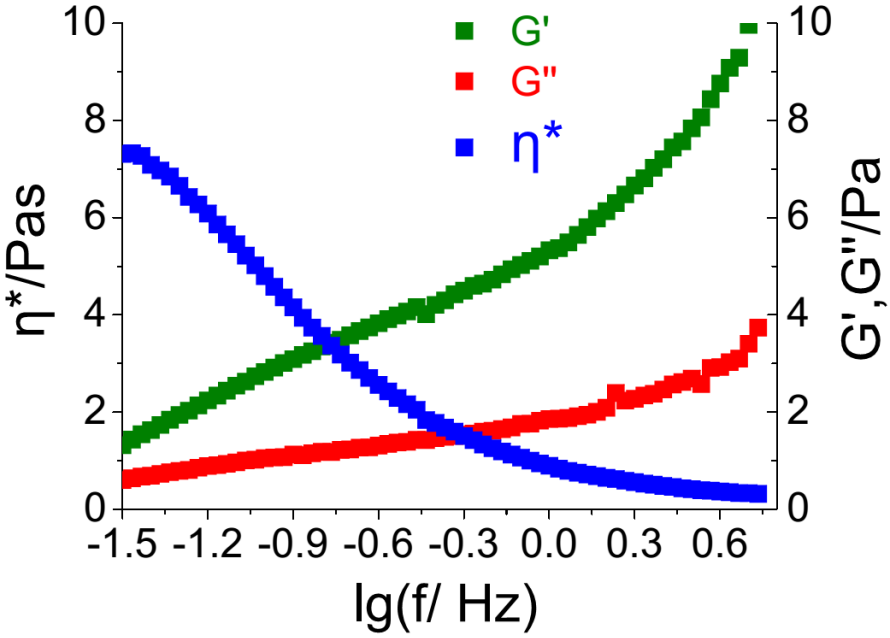

Figure S9. Dynamic frequency sweep rheometry data for metallo-hydrogel [**2**+Cys] (0.5 wt%) at 25 °C (angular frequency from 0.005–20 rad s¯1, strain kept at 0.8 % without deformation, storage modulus (G') > loss modulus (G''), η*: complex viscosity)

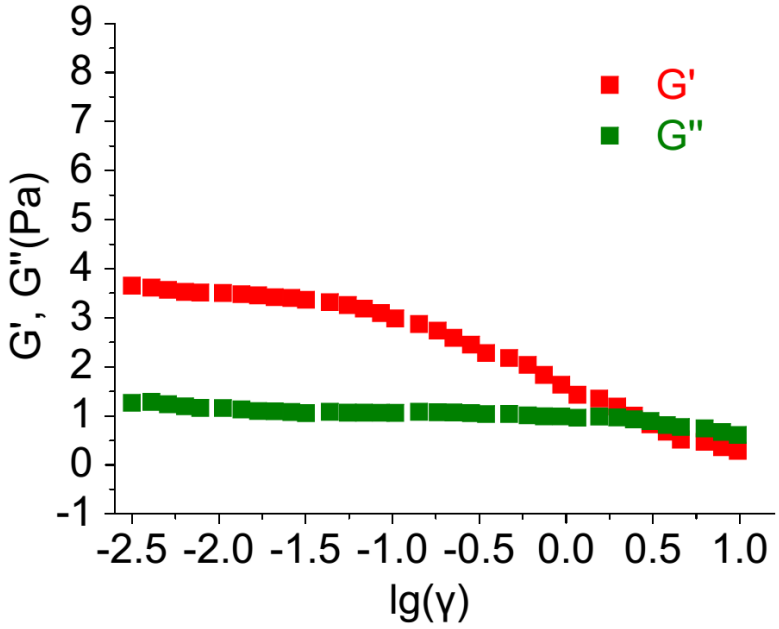

Figure S10. Amplitude sweep rheometry data (storage modulus G' and loss modulus G'' *vs.* shear strain γ) for metallo-hydrogel [**2**+Hcy] (0.5 wt%) at 25 ^{o}C (angular frequency: 6.283 rad s^{-}1, strain: 0.001–10).

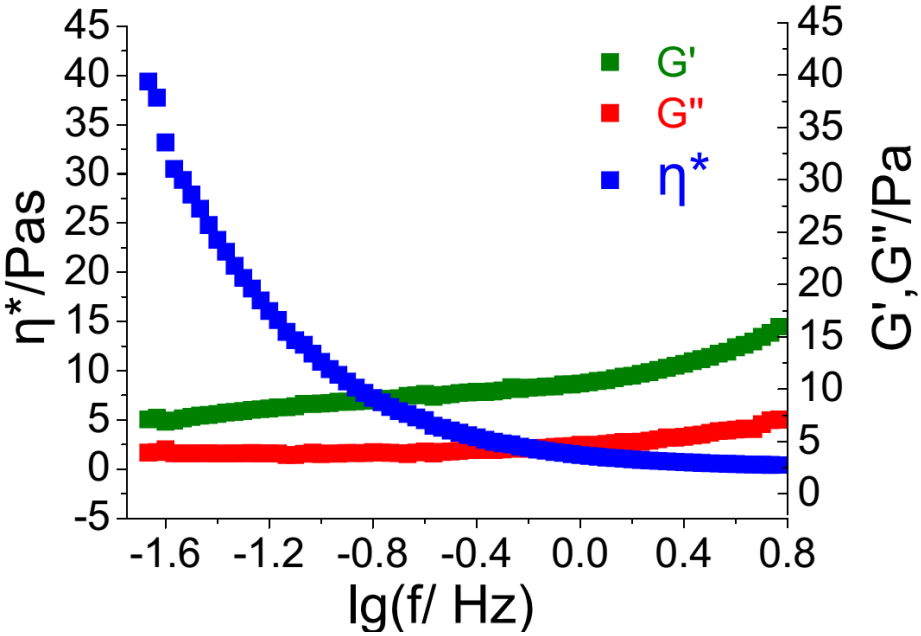

Figure S11. Dynamic frequency sweep rheometry data for metallo-hydrogel [**2**+Hcy] (0.5 wt%) at 25 ^{o}C (angular frequency from 0.005–20 rad s^{-}1, strain kept at 0.8 % without deformation, storage modulus (G') > loss modulus (G''), η*: complex viscosity)

12. SEM Morphologies.

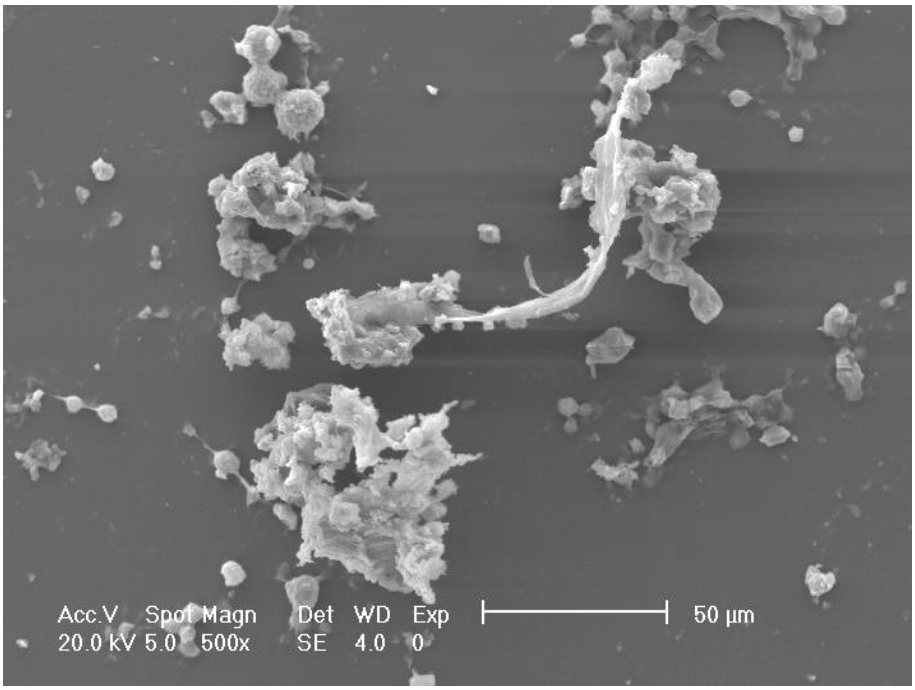

Figure S12. SEM image of precipitates (0.4 wt%) formed by complex **2** in H_2O, scale of bar 50 µm.

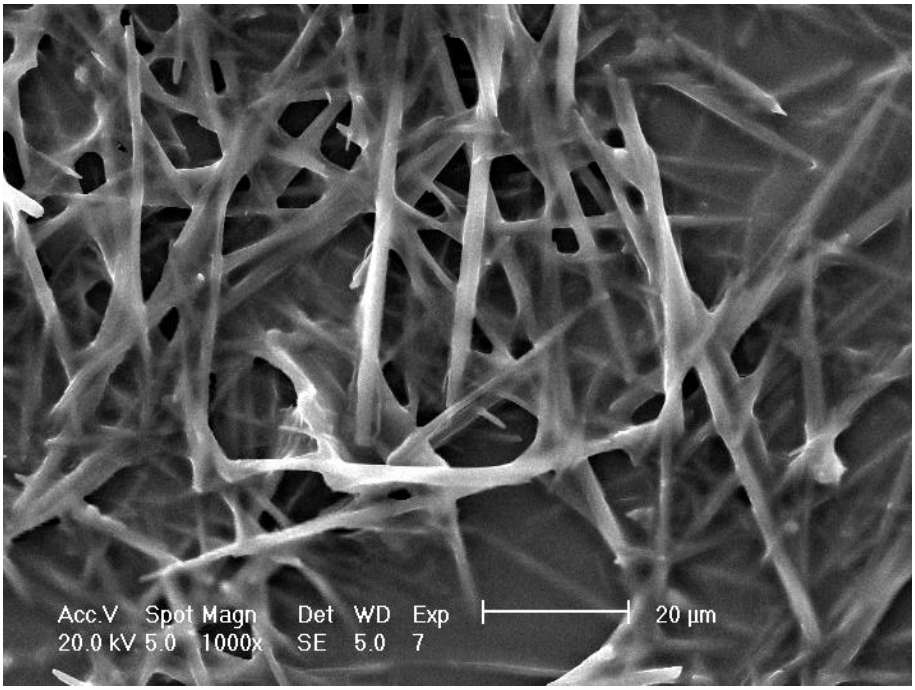

Figure S13. SEM image of metallogel (1.0 wt%) formed by complex **2** in glycerin, scale of bar 20 µm.

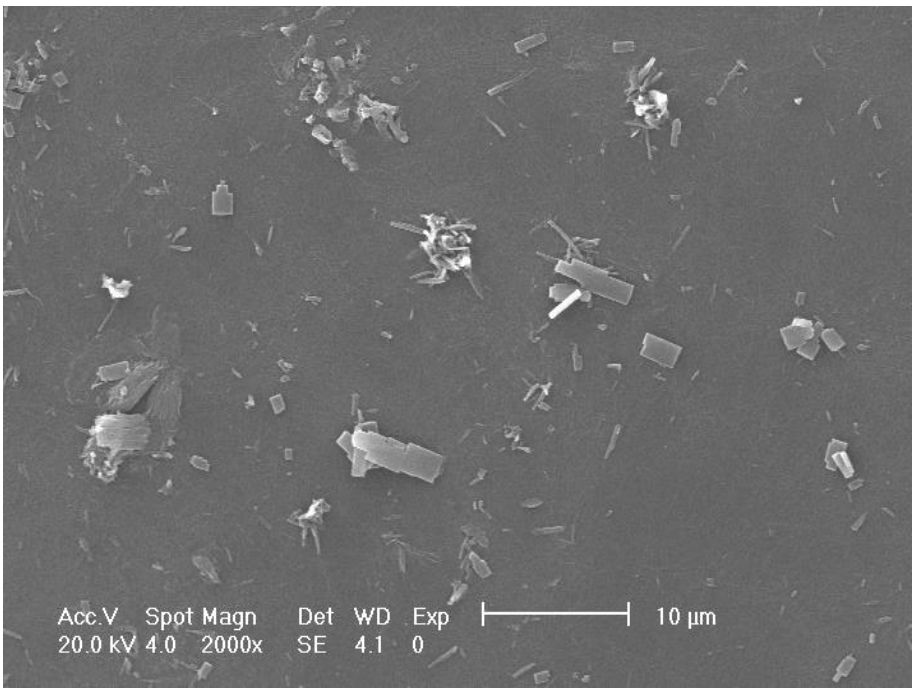

Figure S14. SEM image of precipitate (0.4 wt%) formed by complex **2** with 2 eq. L-Ala in H_2O, scale of bar 10 µm.

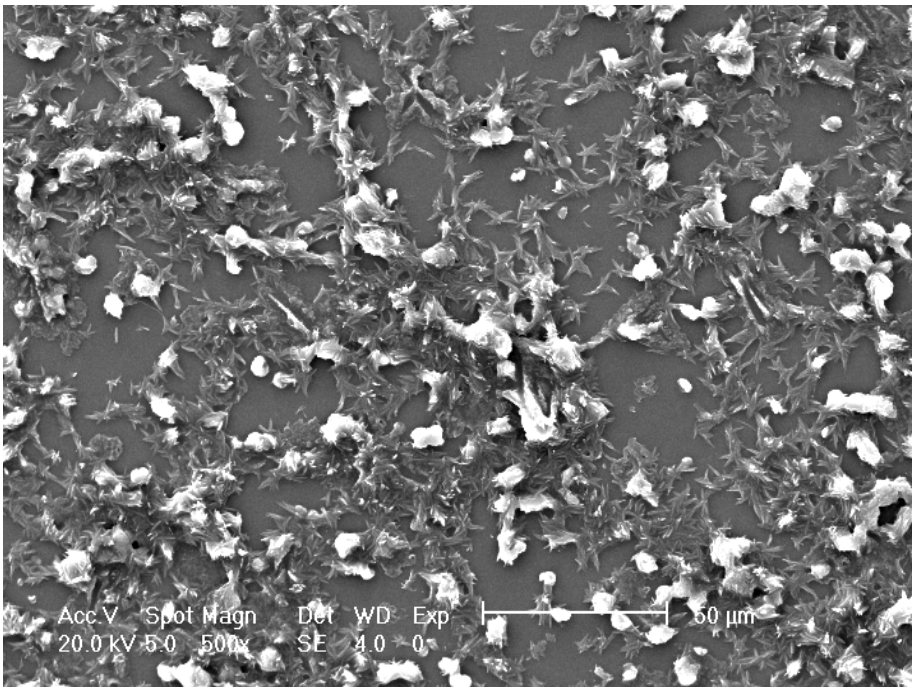

Figure S15. SEM image of precipitate (0.4 wt%) formed by complex **2** with 2 eq. L-Arg in H_2O, scale of bar 50 µm.

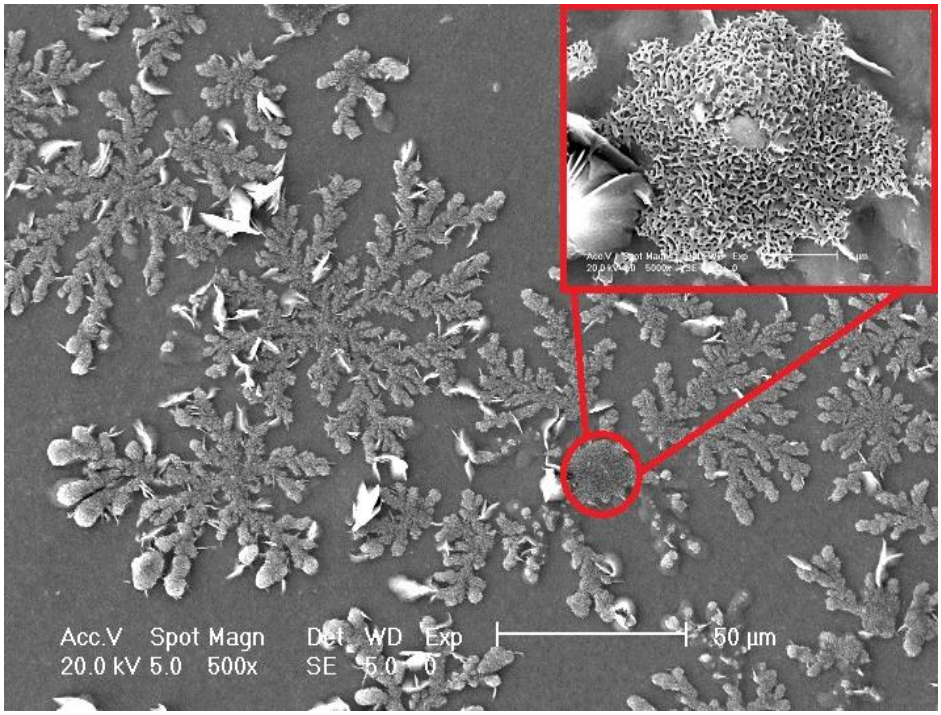

Figure S16. SEM image of metallo-hydrogel [**2**+Cys] (0.4 wt%) formed by complex **2** with 2 eq. L-Cys in H_2O, scale of bar 50 µm.

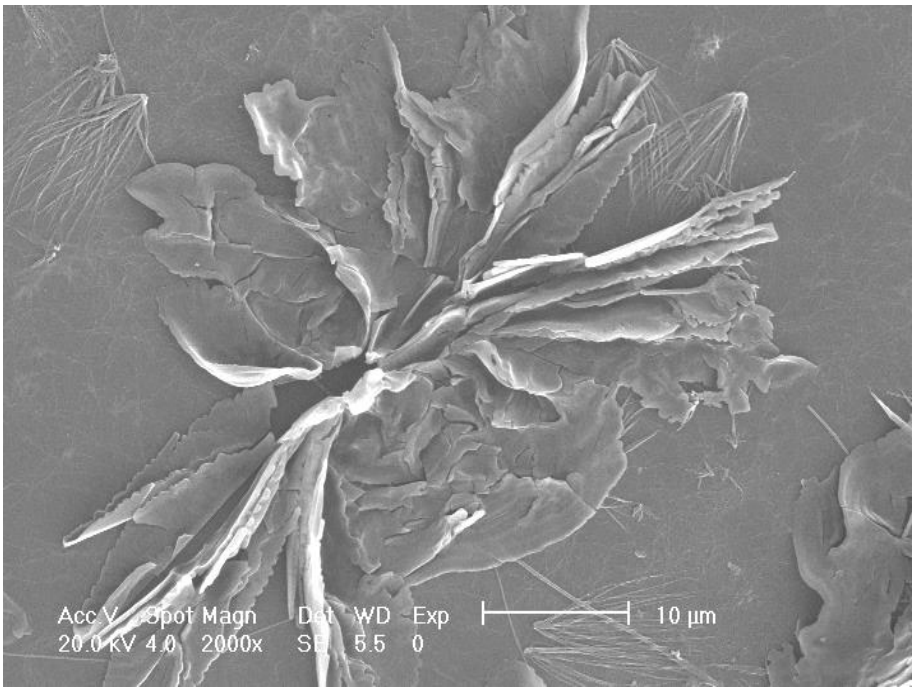

Figure S17. SEM image of precipitate (0.4 wt%) formed by complex **2** with 2 eq. L-Cystine in H_2O, scale of bar 10 µm.

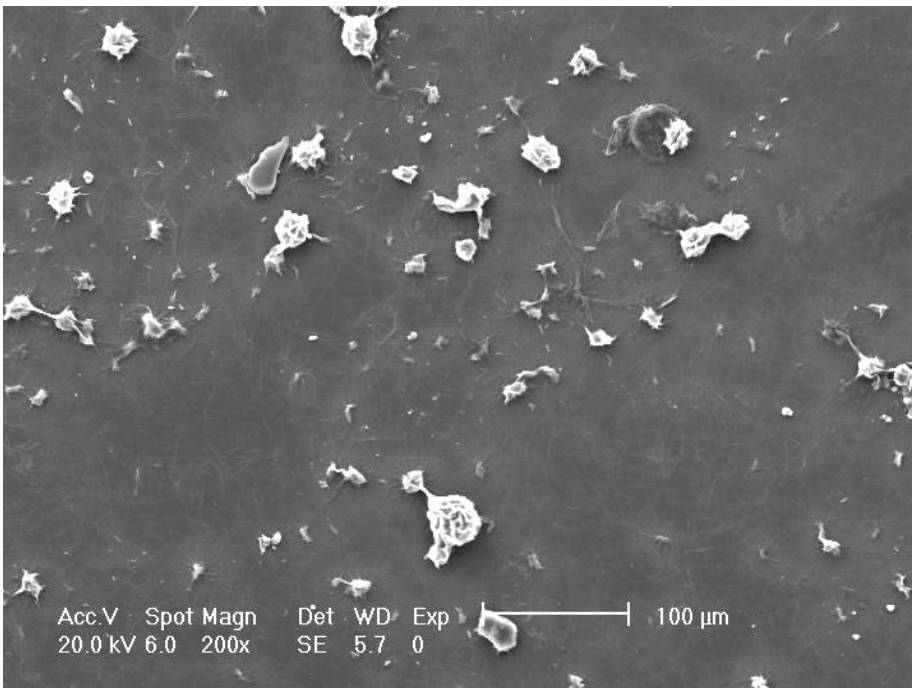

Figure S18. SEM image of precipitate (0.4 wt%) formed by complex **2** with 2 eq. L-Glu in H_2O, scale of bar 100 µm.

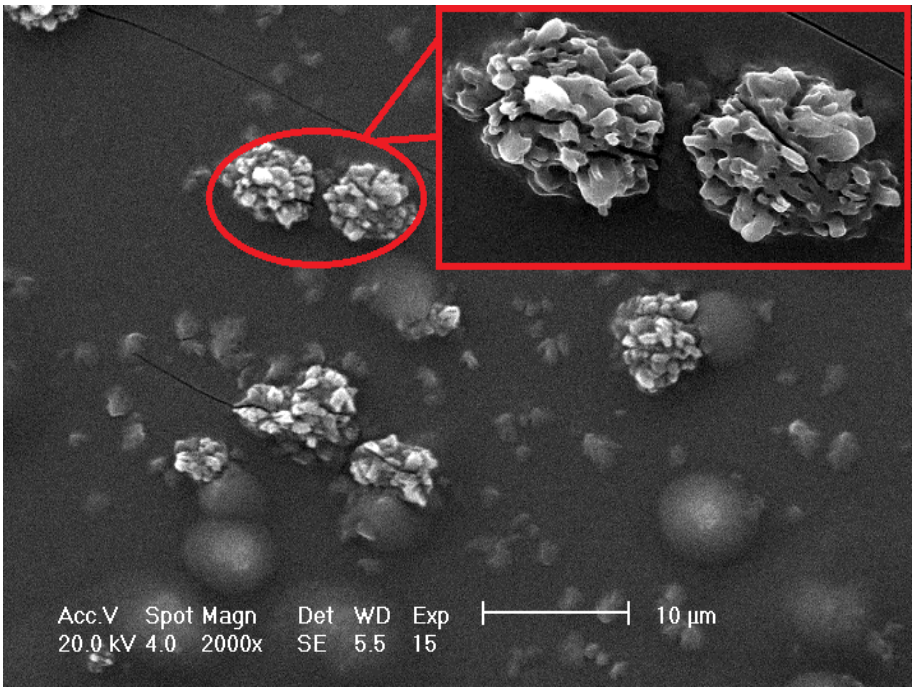

Figure S19. SEM image of metallo-hydrogel [**2**+Hcy] (0.4 wt%) formed by complex **2** with 2 eq. L-Hcy in H_2O, scale of bar 10 µm.

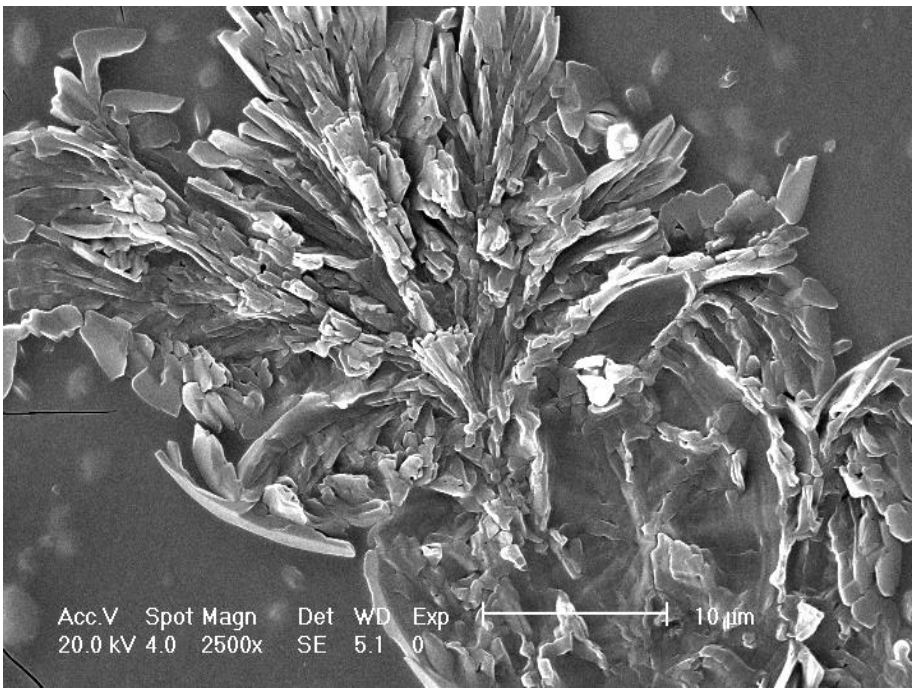

Figure S20. SEM image of solvent (0.4 wt%) formed by complex **2** with 2 eq. L-His in H_2O, scale of bar 10 µm.

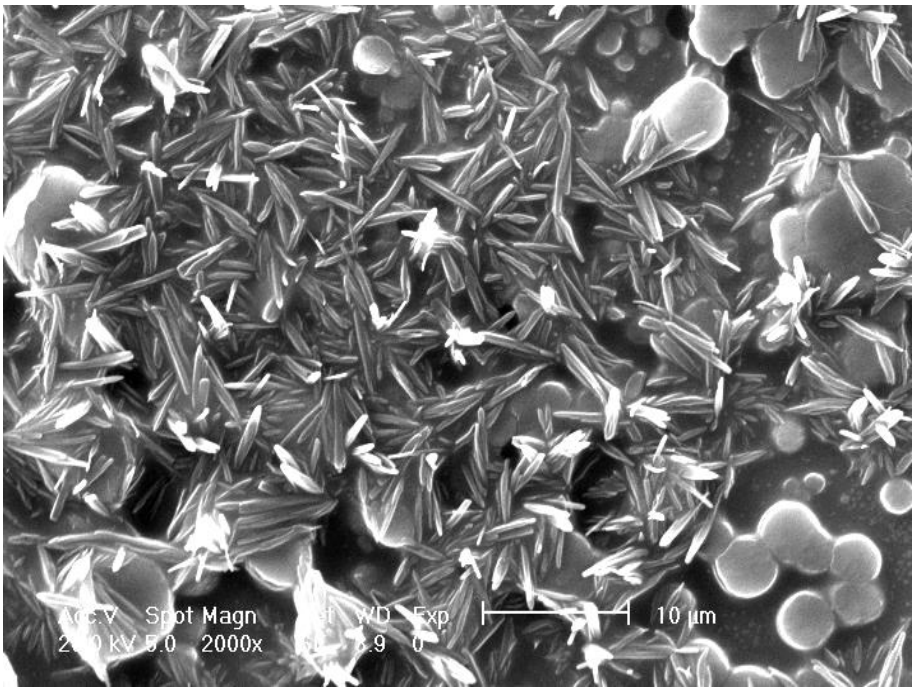

Figure S21. SEM image of precipitate (0.4 wt%) formed by complex **2** with 2 eq. L-Lys in H_2O, scale of bar 10 µm.

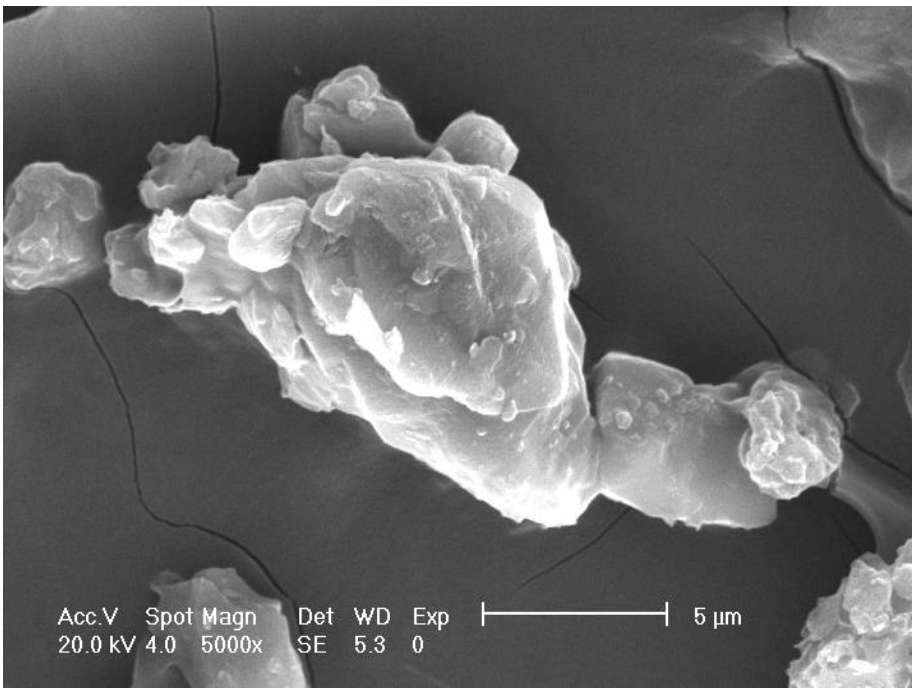

Figure S22. SEM image of precipitate (0.4 wt%) formed by complex **2** with 2 eq. L-Met in H_2O, scale of bar 5 µm.

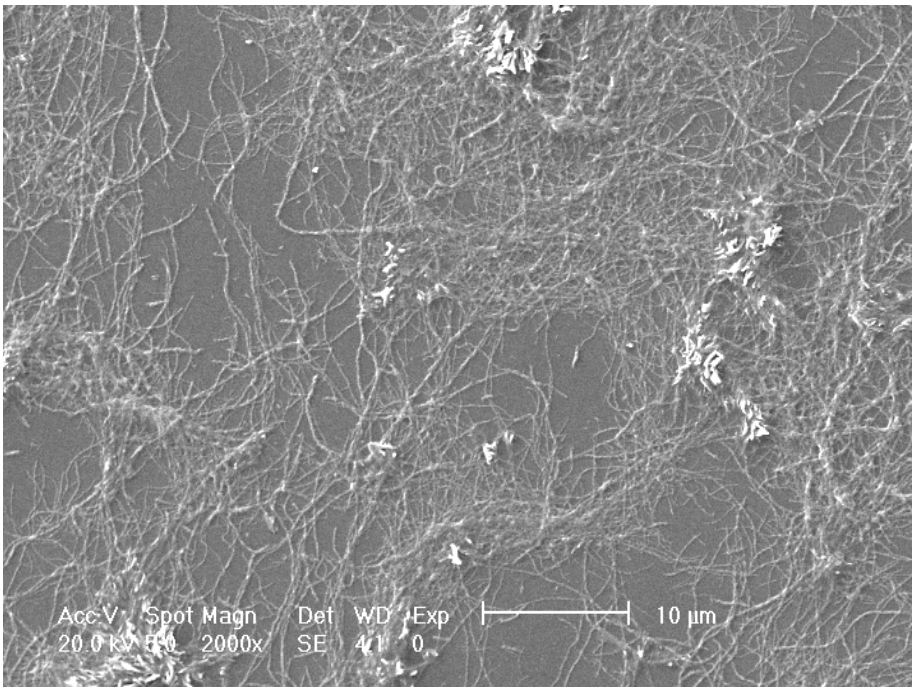

Figure S23. SEM image of precipitate (0.4 wt%) formed by complex **2** with 2 eq. D-Phe in H_2O, scale of bar 10 µm.

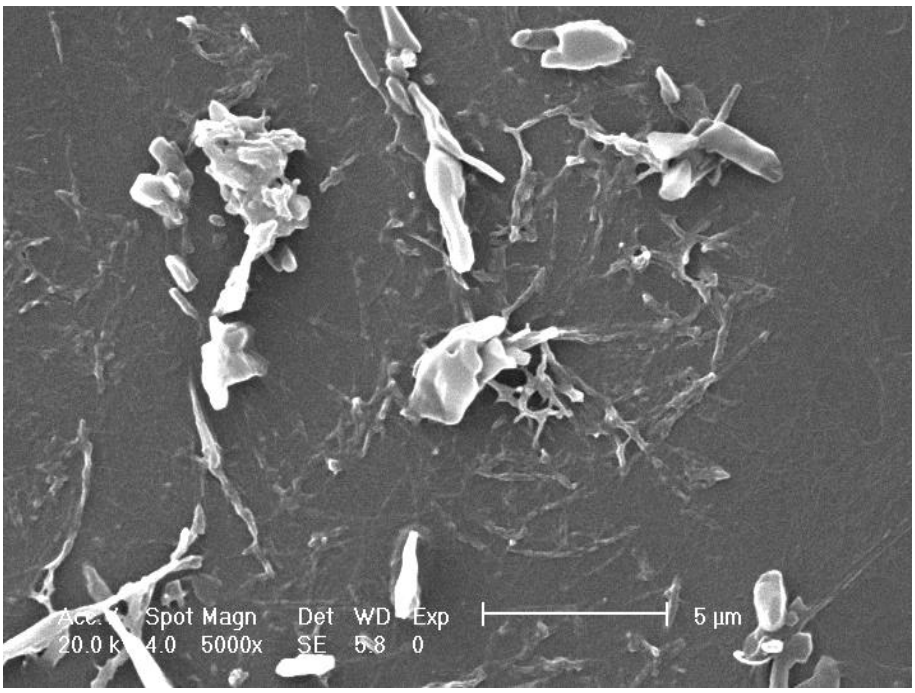

Figure S24. SEM image of precipitate (0.4 wt%) formed by complex **2** with 2 eq. L-Pro in H_2O, scale of bar 5 µm.

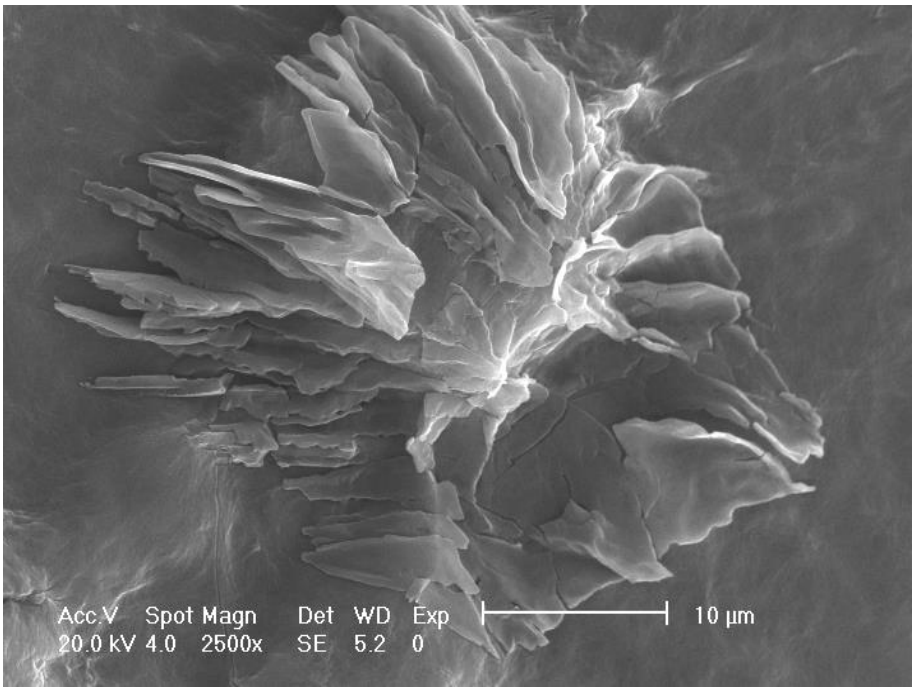

Figure S25. SEM image of precipitate (0.4 wt%) formed by complex **2** with 2 eq. L-Ser in H_2O, scale of bar 10 µm.

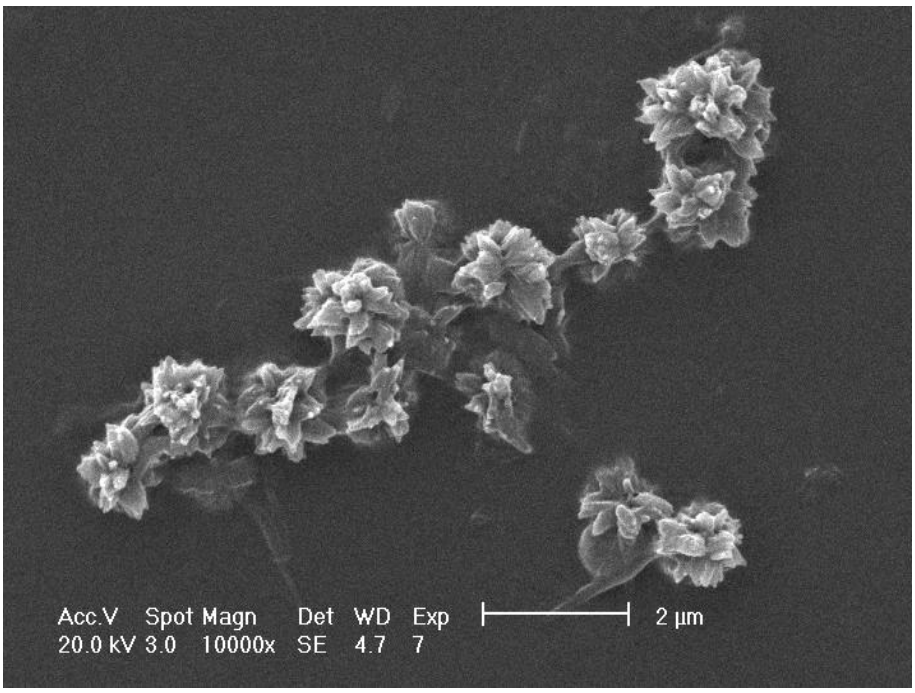

Figure S26. SEM image of metallo-hydrogel [**2**+GSH] (0.5 wt%) formed by complex **2** with 2 eq. GSH in H_2O, scale of bar 2 µm.

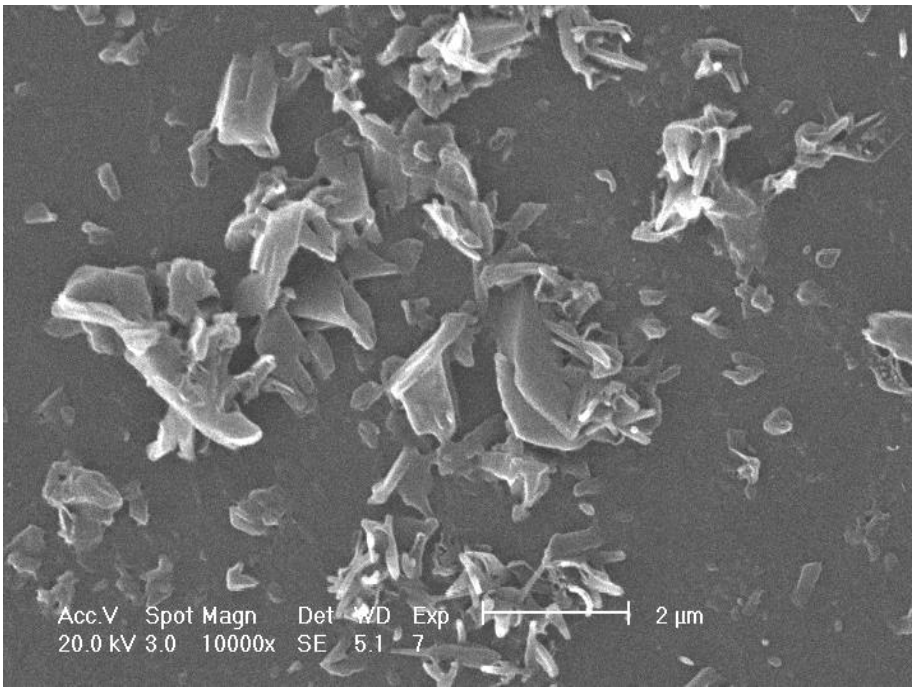

Figure S27. SEM image of precipitate (0.4 wt%) formed by complex **2** with 2 eq. Gly in H_2O, scale of bar 2 µm.

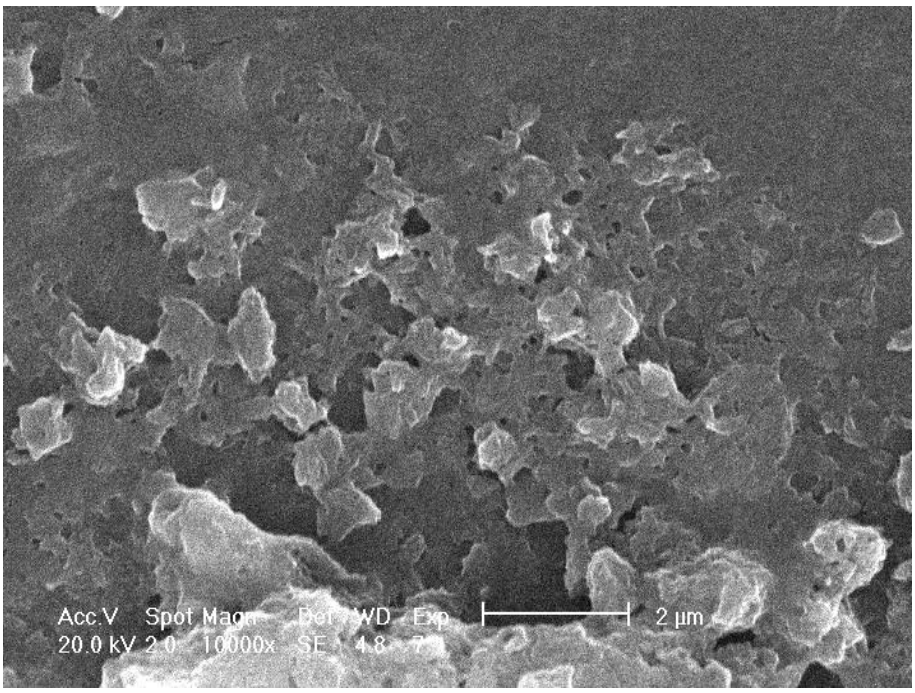

Figure S28. SEM image of metallo-hydrogel (0.4 wt%) formed by complex **2** with 2 eq. 3-MPA in H_2O, scale of bar 2 µm.

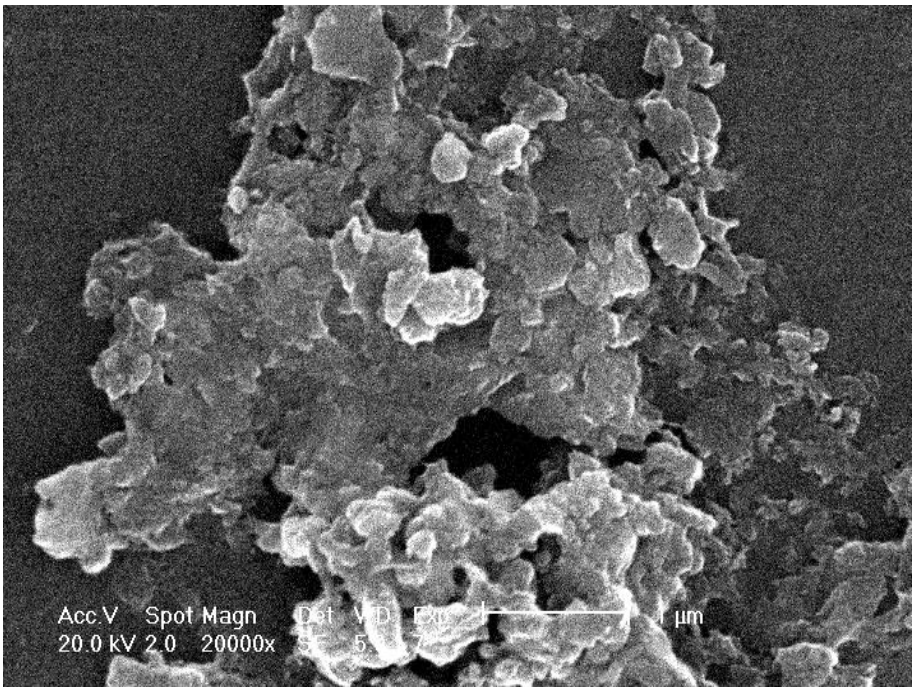

Figure S29. SEM image of metallo-hydrogel (0.4 wt%) formed by complex **2** with 2 eq. 3-MPE in H_2O, scale of bar 1 µm.

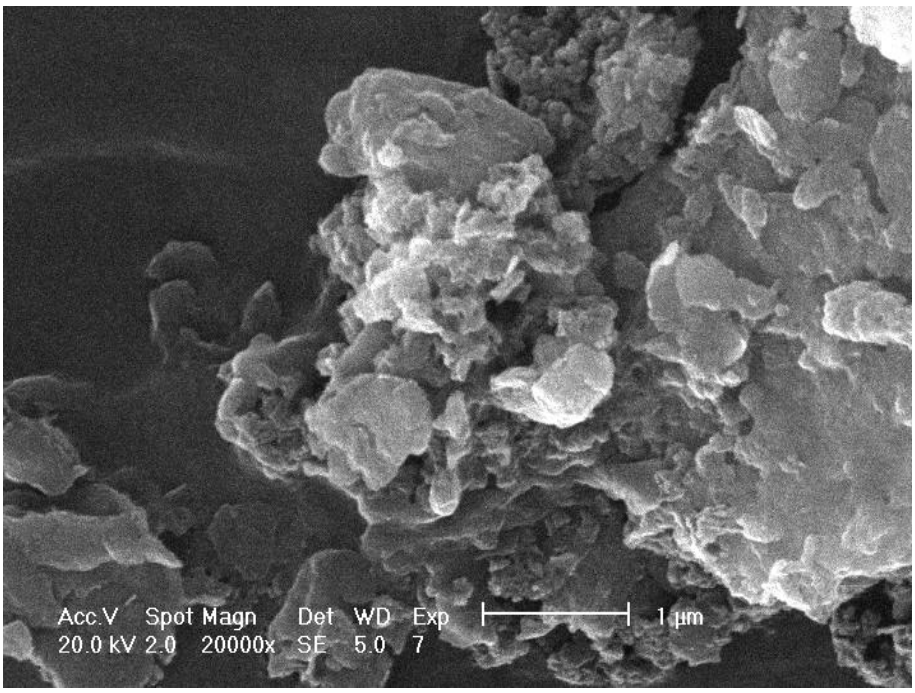

Figure S30. SEM image of metallo-hydrogel (0.4 wt%) formed by complex **2** with 2 eq. butyl mercaptan in H_2O, scale of bar 1 µm.

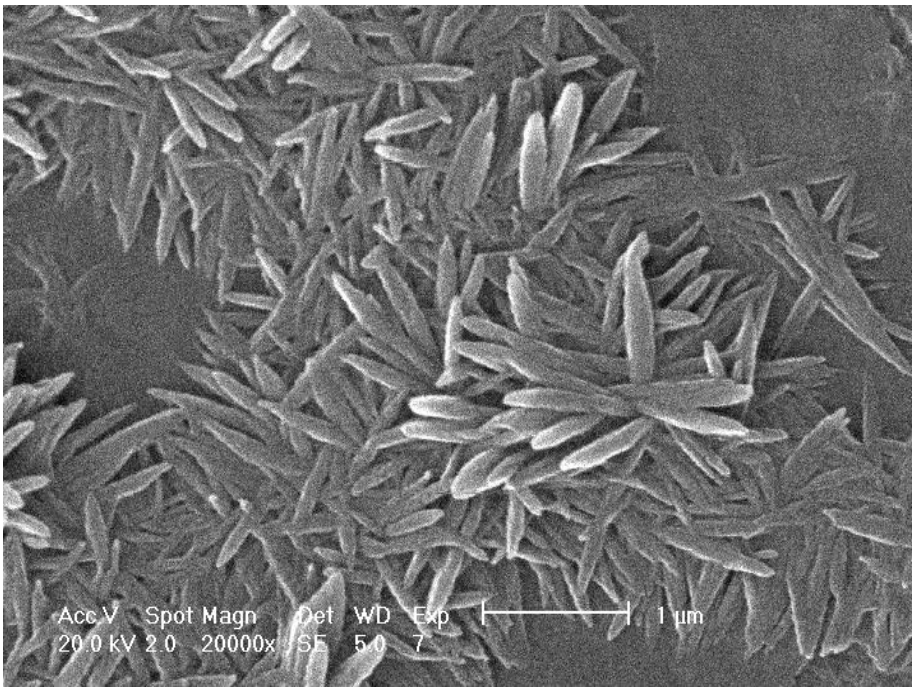

Figure S31. SEM image of precipitate (0.4 wt%) formed by complex **2** with 2 eq. benzyl mercaptane in H_2O, scale of bar 1 µm.

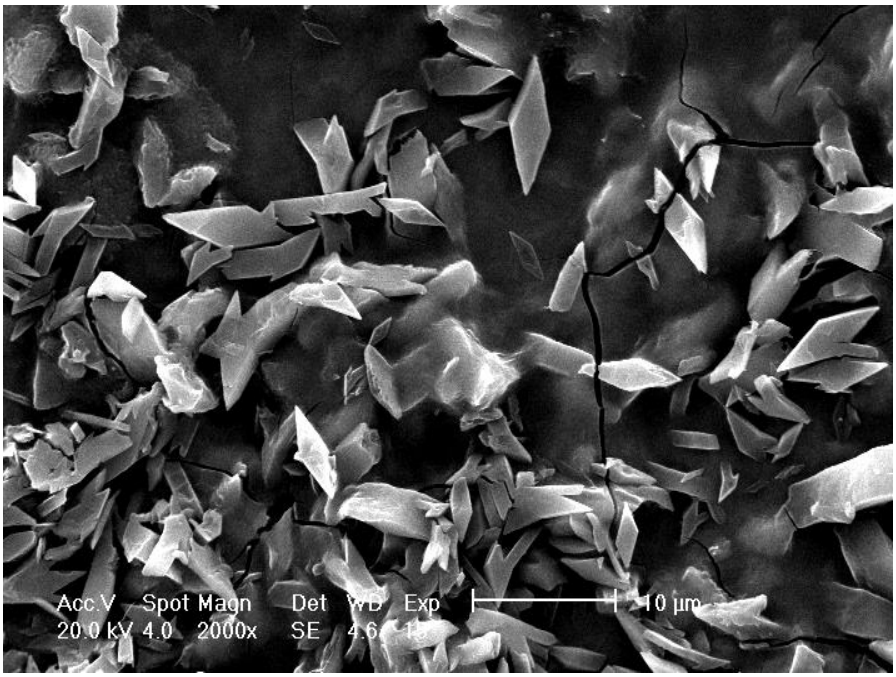

Figure S32. SEM image of collapsed sol formed by the metallo-hydrogel [**2**+Cys] (0.4 wt%) after the addition of 0.4 eq. EDTA, scale of bar 10 µm.

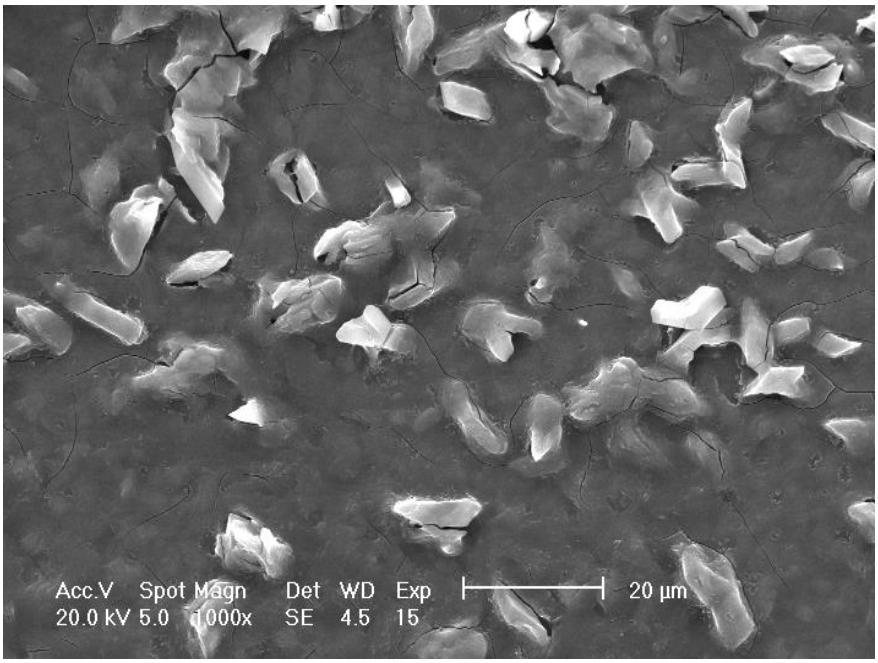

Figure S33. SEM image of collapsed sol formed by the metallo-hydrogel [**2**+Hcy] (0.4 wt%) after the addition of 0.4 eq. EDTA, scale of bar 20 µm.

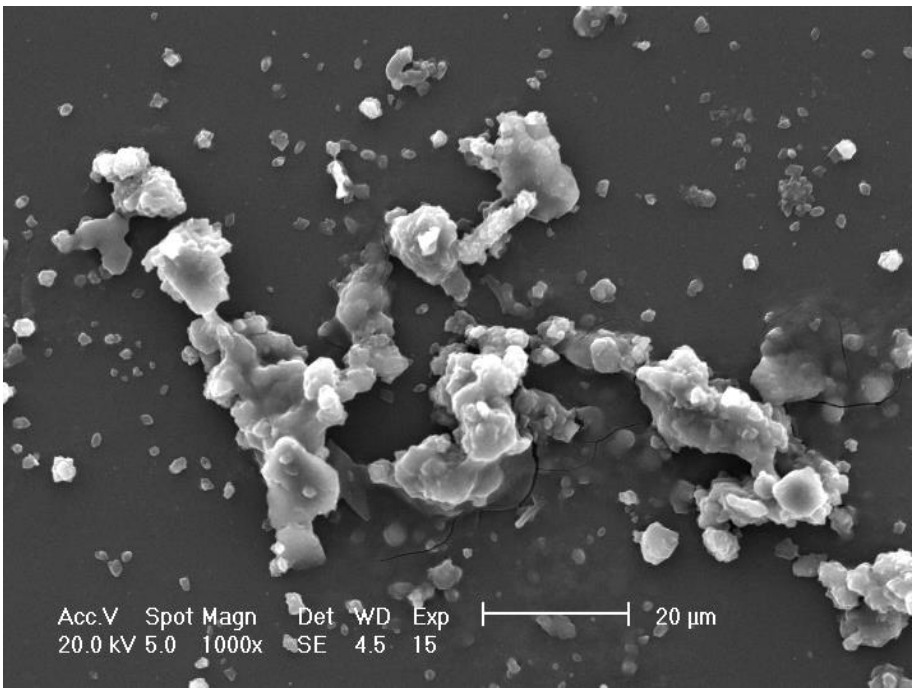

Figure S34. SEM image of collapsed sol formed by the metallo-hydrogel [**2**+GSH] (0.5 wt%) after the addition of 0.4 eq. EDTA, scale of bar 20 µm.

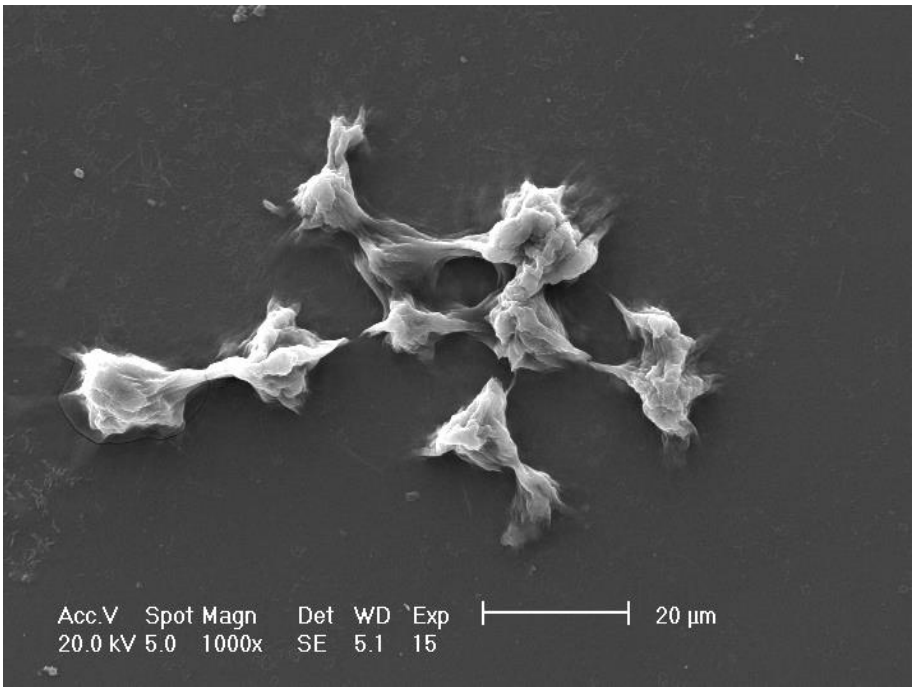

Figure S35. SEM image of precipitate formed by the collapsed sol [(**2**+Cys) + 0.4 eq. EDTA] (0.4 wt%) after the addition of 0.4 eq. $ZnCl_2$, scale of bar 20 µm.

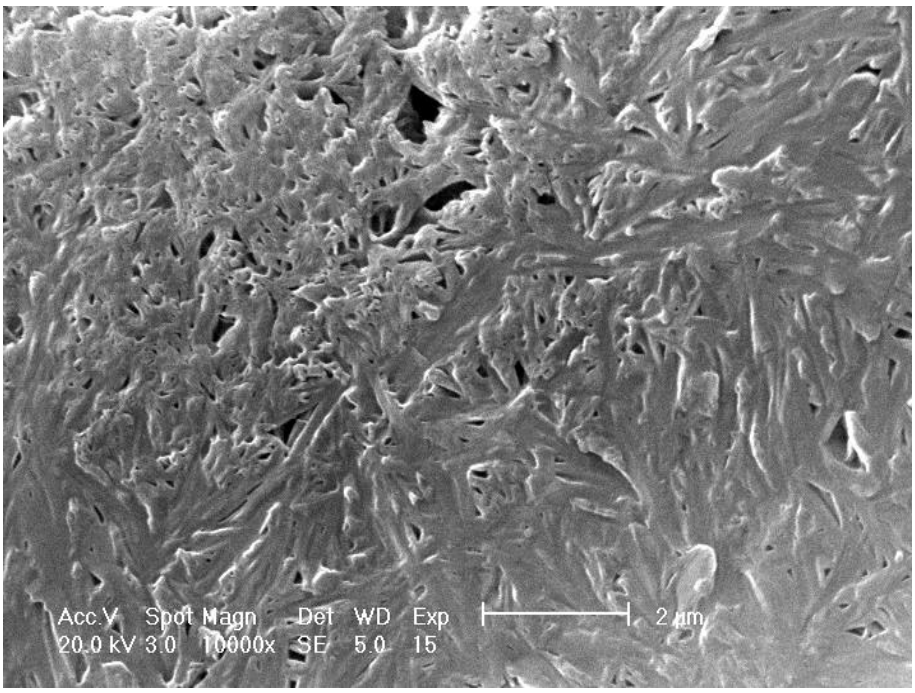

Figure S36. SEM image of metallo-hydrogel reformed by the collapsed sol [(**2**+Hcy) + 0.4 eq. EDTA] (0.4 wt%) after the addition of 0.4 eq. $ZnCl_2$, scale of bar 2 µm.

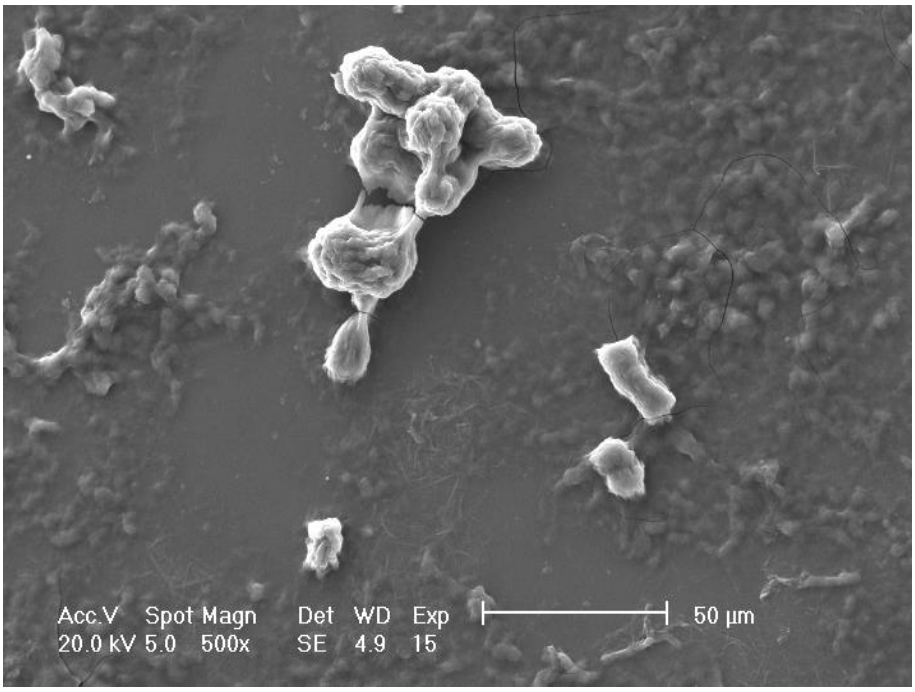

Figure S37. SEM image of precipitate formed by the collapsed sol [(**2**+GSH) +0.4 eq. EDTA] (0.5 wt%) after the addition of 0.4 eq. $ZnCl_2$, scale of bar 10 µm.

13. Circular dichroism (CD) studies.

In order to test whether chiral molecules are able to accelerate the gel formation, circular dichroism (CD) spectroscopy was then applied for further characterization. An aqueous solution of complex **2** (9.2×10^{-3} M) revealed no obvious CD signal from 360 nm to 450 nm region (Fig. S38). A similar phenomenon was encountered with the hot sol [**2**+Hcy]/H_2O (molar ratio: 1:2, 9.2×10^{-3} M). Interestingly, a strong positive Cotton effect at 375 nm could be observed with the gel [**2**+Hcy]/H_2O (0.4 wt%) with a split at [θ] = 0 line. Therefore, a more detailed chiroptical study on the gelation was performed (Fig. S39). Although the hot sol [**2**+Hcy]/H_2O (molar ratio: 1:2, 9.2×10^{-3} M) exhibited no CD signals, a broad CD signal at 375 nm appeared and gradually increased in intensity during the sample cooling. The chiral amplification phenomenon observed during the gel formation indicated that the amino acid was involved in the molecular assembly and that mercapto molecules coordinate to complex **2** leading to the gel formation. A similar outcome was found for the formation of gel [**2**+Cys]/H_2O; the intensity of the CD signal, however, was lower than that of [**2**+Hcy]/H_2O at the same concentration suggesting that adducts formed from complex **2** and Hcy are packed more densely resulting in a more stable gel. The collapsed sols [(**2**+Hcy)+EDTA]/H_2O and [(**2**+Cys)+EDTA]/H_2O did not reveal any CD signal in the region of 360 - 450 nm supporting the idea that the CD signals observed in the gel state arise from the molecular assembly by adducts formed from complex **2** and the thiols. The reformed gel prepared from sol [(**2**+Hcy)+EDTA]/H_2O and 0.4 eq. $ZnCl_2$ did not reveal any CD signal. We proposed that the Zn^{2+}-EDTA complex may affect the gel assembly packing model *via* metal–metal interaction with adducts formed from complex **2** and the thiol, although the detail mechanism is still under the investigation.

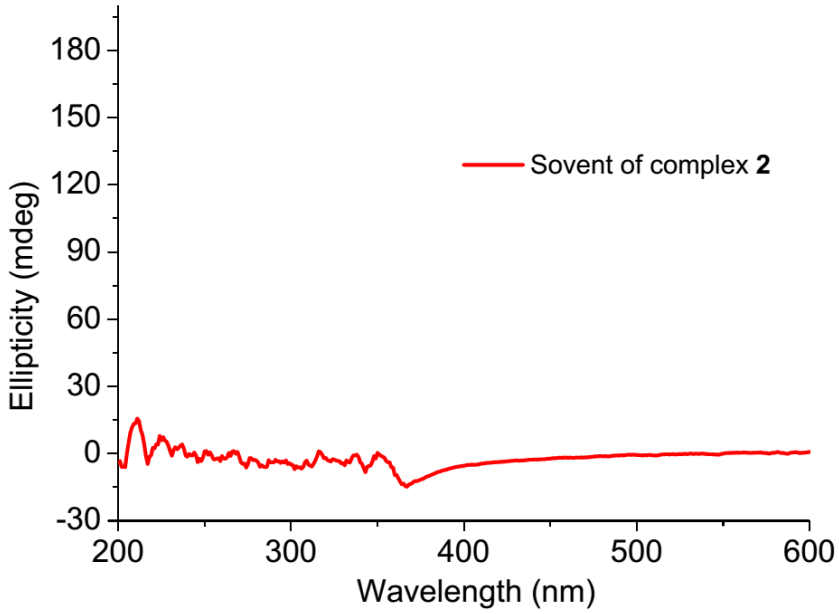

Figure S38. CD spectra of solvent **2** in H_2O (9.2×10^{-3} M).

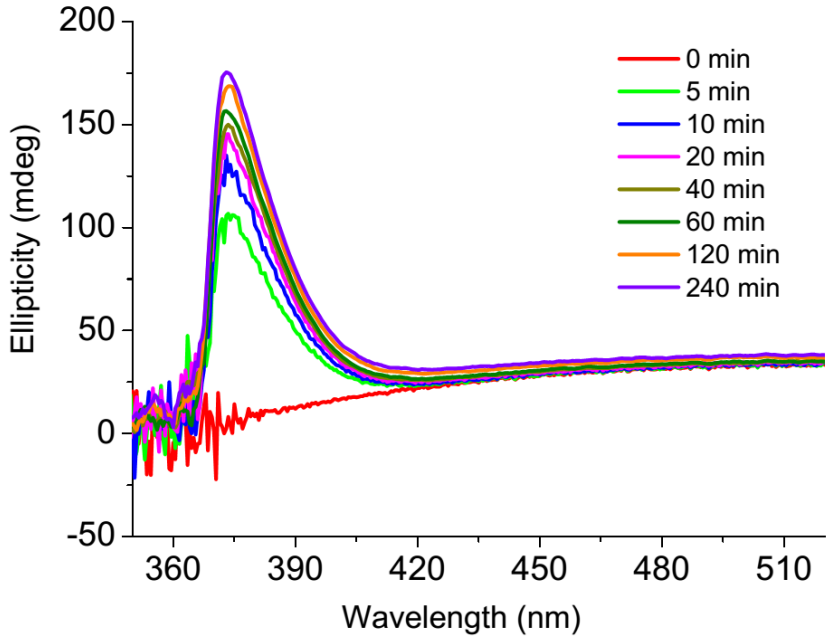

Figure S39. The variation of CD intensity obtained during the transformation from the hot sol to metallo-hydrogel [**2**+Hcy] (0.4 wt%).

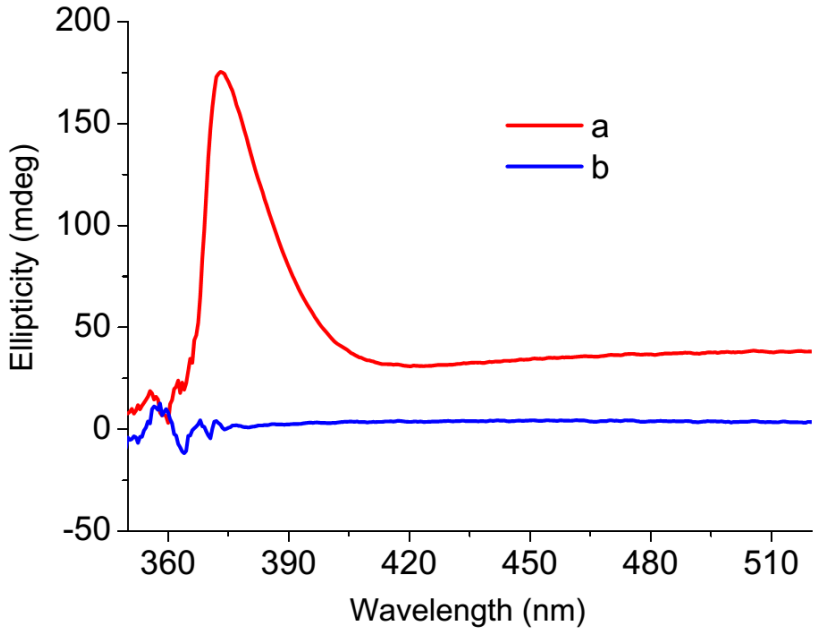

Figure S40. CD spectra of: a) metallo-hydrogel [**2**+Hcy] (0.4 wt%) and b) collapsed sol formed by metallo-hydrogel [**2**+Hcy] (0.4 wt%) after the addition of 0.4 eq. EDTA.

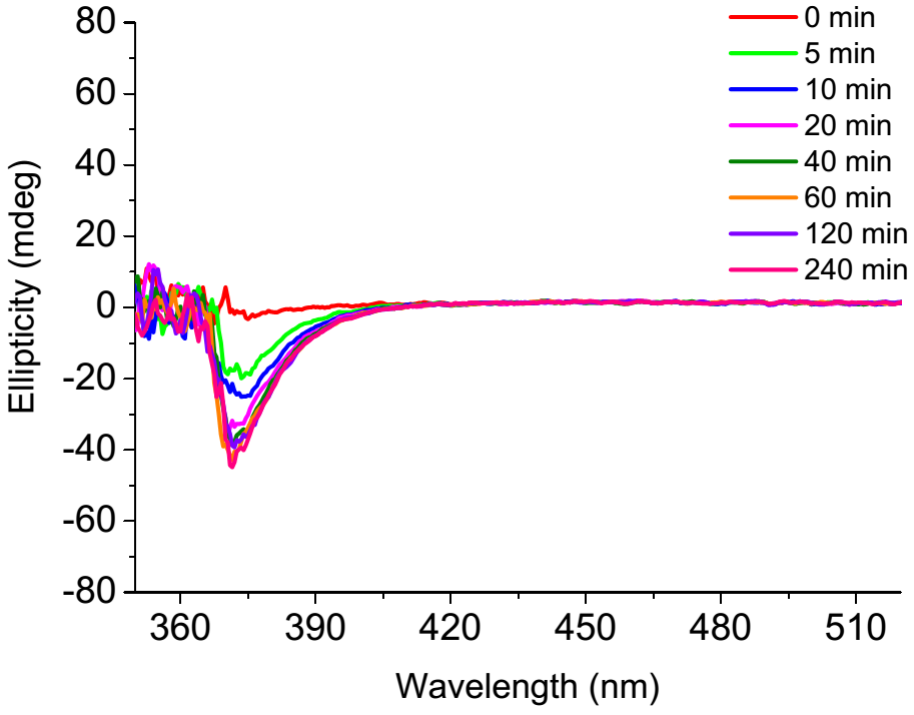

Figure S41. The variation of CD intensity obtained during the transformation from the hot sol to metallo-hydrogel [**2**+Cys] (0.4 wt%).

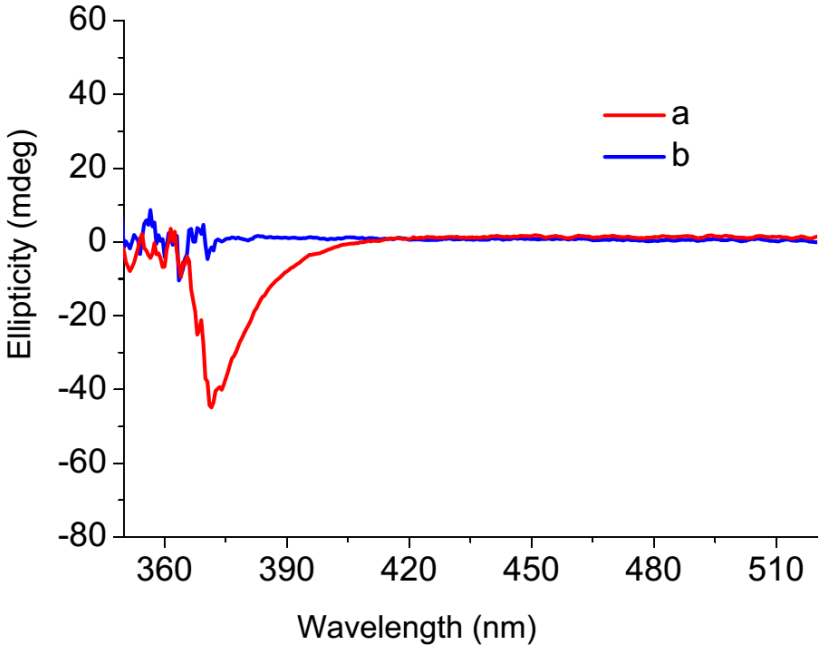

Figure S42. CD spectra of: a) metallo-hydrogel [**2**+Cys] (0.4 wt%) and b) collapsed sol formed by metallo-hydrogel [**2**+Cys] (0.4 wt%) after the addition of 0.4 eq. EDTA.

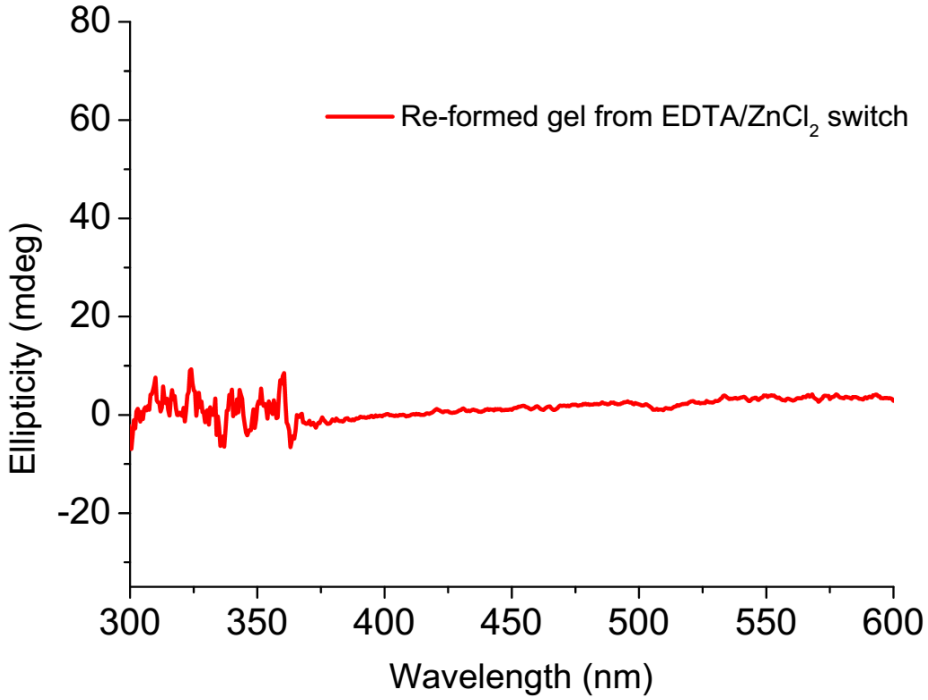

Figure S43. CD spectra of metallo-hydrogel reformed by the collapsed sol [**2**+Hcy] (0.4 wt%) containing 0.4 eq. EDTA after the addition of 0.4 eq. $ZnCl_2$.

14. NMR and ESI-MS spectra for Complex 2.

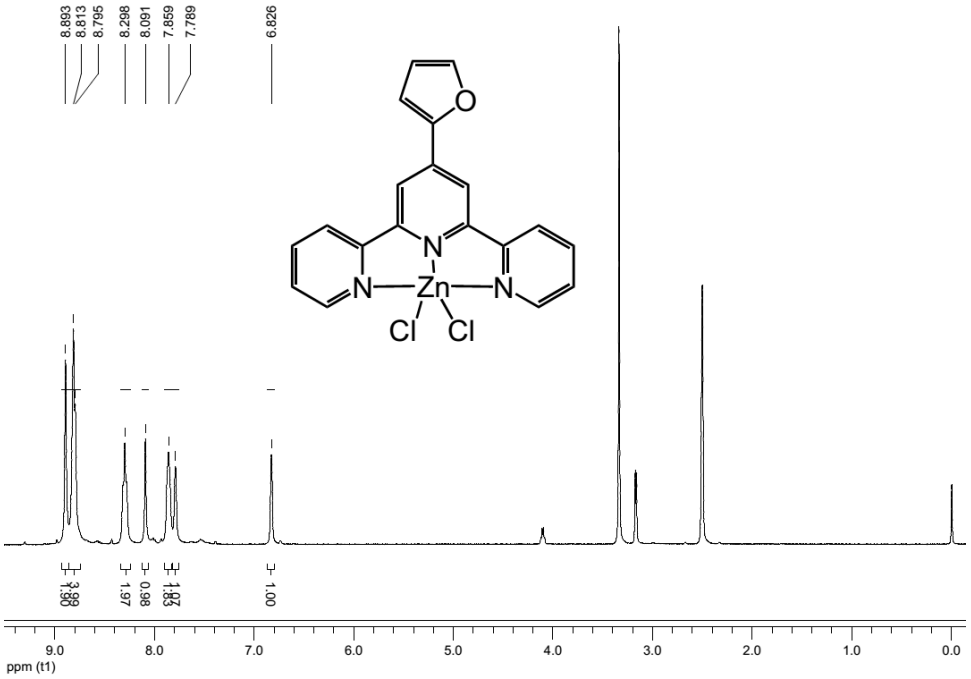

Figure S44. ^{1}H NMR (DMSO-D_6, 400 MHz, 298 K) spectrum of complex **2**.

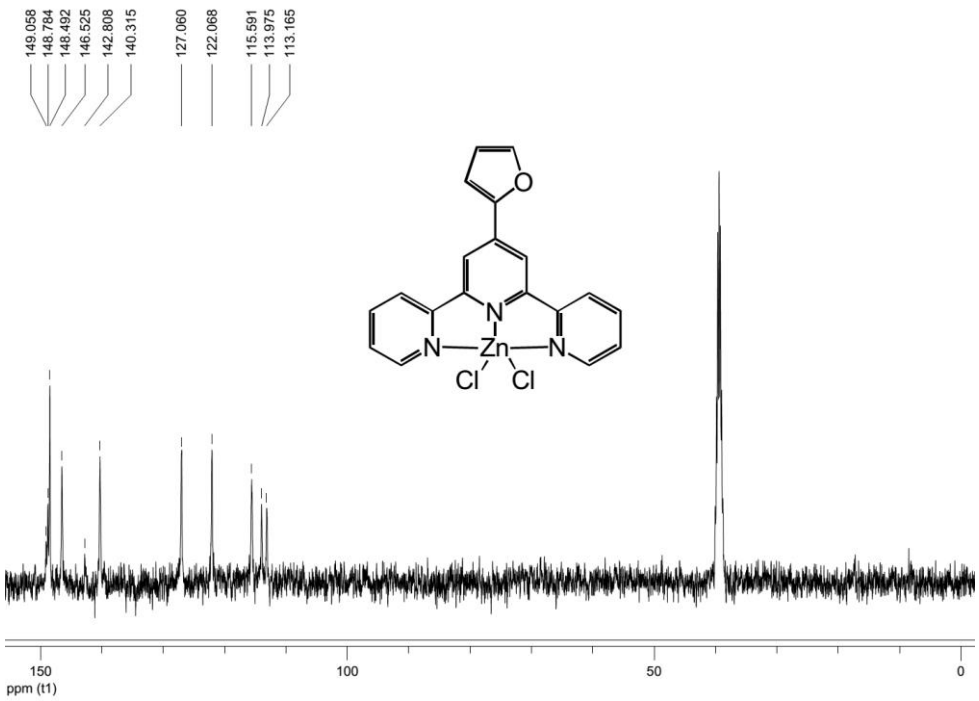

Figure S45. ^{13}C NMR (DMSO-D_6, 100 MHz, 298 K) spectrum of complex **2**.

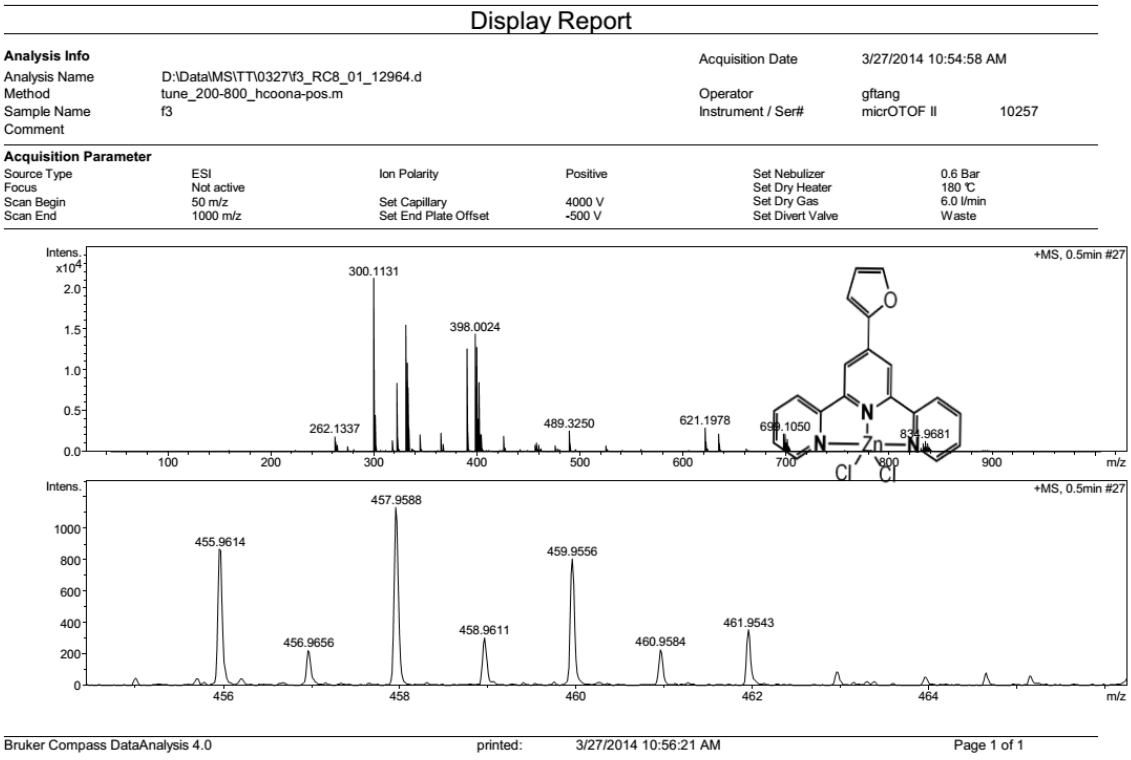

Figure S46. ESI-MS spectrum of complex **2**.

15. References.

S1 K. Murata, M. Aoki, T. Suzuki, T. Harada, H. Kawabata, T. Komori, K. Ueda and S, Shinkai, *J. Am. Chem. Soc.*, 1994, **116**, 6664.

S2 W. Fang, Z. Sun and T. Tu, *J. Phys. Chem. C*, 2013, **117**, 25185.

S3 G. Yu, X. Yan, C. Han and F. Huang, *Chem. Soc. Rev.*, 2013, **42**, 6697.